

# NJC

Accepted Manuscript



This is an *Accepted Manuscript*, which has been through the Royal Society of Chemistry peer review process and has been accepted for publication.

*Accepted Manuscripts* are published online shortly after acceptance, before technical editing, formatting and proof reading. Using this free service, authors can make their results available to the community, in citable form, before we publish the edited article. We will replace this *Accepted Manuscript* with the edited and formatted *Advance Article* as soon as it is available.

You can find more information about *Accepted Manuscripts* in the [Information for Authors](#).

Please note that technical editing may introduce minor changes to the text and/or graphics, which may alter content. The journal's standard [Terms & Conditions](#) and the [Ethical guidelines](#) still apply. In no event shall the Royal Society of Chemistry be held responsible for any errors or omissions in this *Accepted Manuscript* or any consequences arising from the use of any information it contains.

## Theoretical and experimental characterization of a novel pyridine benzimidazole: Suitability for fluorescence staining in cells and antimicrobial properties.†

Alexander Carreño<sup>1,2\*</sup>, Manuel Gacitúa<sup>3</sup>, Juan A. Fuentes<sup>4</sup>, Dayán Páez-Hernández<sup>1,2</sup>, Carmen Araneda<sup>5</sup>, Ivonne Chávez<sup>5,2</sup>, Marco Soto-Arriaza<sup>6</sup>, Juan M. Manríquez<sup>7,2</sup>, Rubén Polanco<sup>8</sup>, Guido C. Mora<sup>9</sup>, Carolina Otero<sup>10</sup>, Wesley B. Swords<sup>11</sup>, Ramiro Arratia-Pérez<sup>1,2</sup>

1. Doctorado en Físicoquímica Molecular, Center of Applied Nanosciences (CENAP), Universidad Andres Bello, Ave. República 275, Santiago, Chile
2. Núcleo Milenio de Ingeniería Molecular para Catálisis y Biosensores (MECB), ICM, Chile
3. Center of Applied Ecology and Sustainability (CAPES), Universidad Adolfo Ibáñez, Peñalolén, Chile
4. Laboratorio de Microbiología, Facultad de Ciencias Biológicas, Universidad Andres Bello, República 217, Santiago, Chile.
5. Departamento de Química Inorgánica, Facultad de Química, Pontificia Universidad Católica de Chile, Avenida Vicuña Mackenna 4860, Santiago, Chile
6. Departamento de Físico-Química, Facultad de Química, Centro de Investigación en Nanotecnología y Materiales Avanzados CIEN-UC, Pontificia Universidad Católica de Chile, Avenida Vicuña Mackenna 4860, Santiago, Chile
7. Laboratorio de Bionanotecnología, Universidad Bernardo O'Higgins, General Gana 1702, Santiago, Chile
8. Facultad de Ciencias Biológicas, Laboratorio de Bioquímica, Universidad Andres Bello, República 217, Santiago, Chile.
9. Laboratorio de Microbiología, Facultad de Medicina, Universidad Andres Bello, Echaurren 183, Santiago, Chile
10. Center for Integrative Medicine and Innovative Science (CIMIS), Facultad de Medicina, Universidad Andres Bello, Echaurren 183, Santiago, Chile.
11. Department of Chemistry, Murray Hall 2202B. University of North Carolina at Chapel Hill, USA.

† *Electronic supplementary information (ESI) available.*

**Abstract.**

Benzimidazoles presenting intramolecular hydrogen bonding interactions have been normally used to better understand the role of H-bonding in biological processes. Here, we present an experimental and theoretical study of a new compound [2,4-di-*tert*-butyl-6-(3H-imidazo[4,5-c]pyridine-2-yl)phenol; (**B2**), a benzimidazole derivate, exhibiting an intramolecular hydrogen bond. **B2** was synthesized and characterized by their  $^1\text{H}$ , HHCOSY, FT-IR and mass spectra (*EI-MS* 323  $\text{M}^+$ ). The electronic and optical properties of **B2** were studied with theoretical calculations using density functional theory (DFT) and time-dependent DFT (TDDFT). **B2** showed luminescent emission at room temperature in different solvents, with a large Stokes shift (e.g.;  $\lambda_{\text{ex}} = 335 \text{ nm}$ ;  $\lambda_{\text{em}} = 510 \text{ nm}$  in acetonitrile). Also, the quantum yield ( $\phi = 0.21$ ) and theoretical band emission are reported. We found that **B2** exhibited a fluorescence emission around 500 nm in ethanol and in acetonitrile, that could be quenched by aqueous solutions of  $\text{Hg}(\text{NO}_3)_2$  in the range of micro molar concentrations. Cyclic voltammetry in acetonitrile showed a strong anodic response due to a quasireversible process, with reduction and oxidation waves at -1.28 and -0.47 V vs SCE. Regarding the biological properties, we assessed the antimicrobial activity of **B2** in *Salmonella enterica* (bacteria), *Cryptococcus* spp. (yeast), *Candida albicans* (yeast), *Candida tropicalis* (yeast) and *Botrytis cinerea* (mold). To this end, we determined the minimal inhibitory concentration (MIC) (for bacteria and yeasts), the growth inhibition halos (for yeasts), and the inhibition of mycelial growth (for the mold). We observed that **B2** exerted an antifungal effect against *Cryptococcus* spp. and *Botrytis cinerea*. In addition, due to its fluorescence property, **B2** has proven to be a suitable marker to observe bacteria (*Salmonella enterica* and an *Escherichia coli* derivative), yeasts (*Candida albicans*), and even human cells (SKOV-3 and HEK-293) by confocal microscopy.

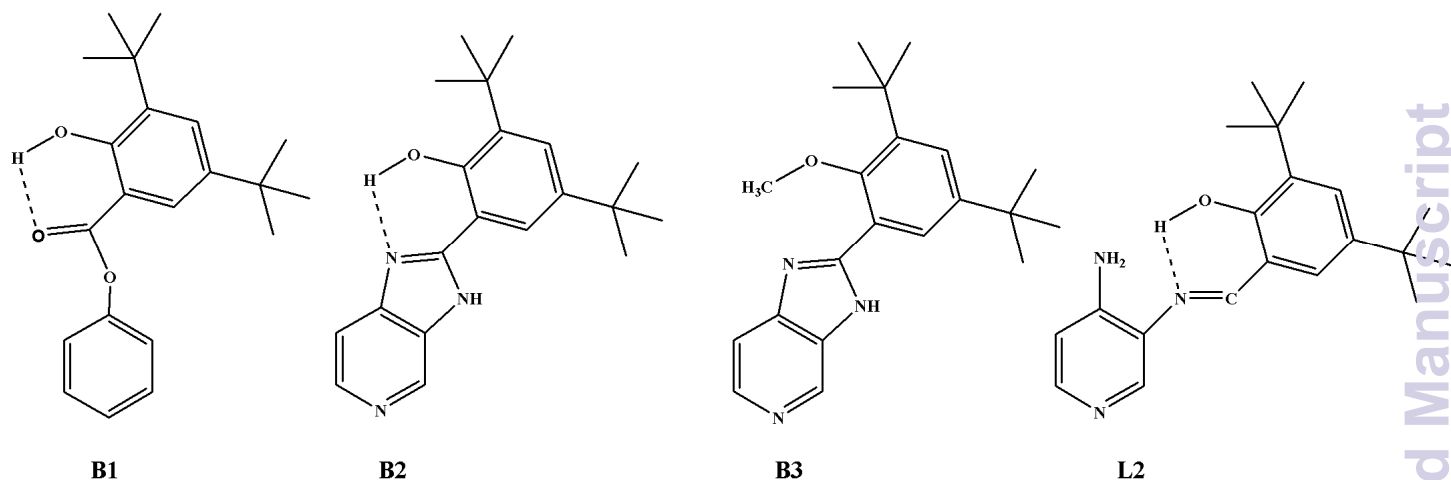
**keywords:** benzimidazole, intramolecular hydrogen bond, DFT, fluorescence quenching, confocal microscopy

## 1. INTRODUCTION

Benzimidazole derivatives are synthetic substances of great medical interest used as constituent of several physiologically active substances, including vitamin B12, and several traditional anthelmintic, antineoplastic, antiviral, antihistaminic, antibacterial, and antifungal products.<sup>1-6</sup> The synthesis of benzimidazoles can be achieved by coupling phenylenediamines and carboxylic acids or their nitriles, imidates, or orthoester derivatives with the reaction of N-ethoxycarbonylthiomides with 1,2-diamines or by reaction of aldehydes with 1,2-diamines, among others.<sup>7-14</sup> The synthesis of benzimidazoles by recyclization reactions has been recently reviewed.<sup>15-19</sup> An important application of benzimidazole compounds is to produce new bioinspired compounds focused into the development of dyes for photoelectrochemical devices, such as, porphyrin macrocycles containing benzimidazole subunits. These structures include a phenol group with an intramolecular hydrogen bond, exhibiting a chemically reversible couple that undergoes photoinduced electron transfer.<sup>20-25</sup>

On the other hand, Schiff bases ligands derived from salicylaldehyde with hydrogen bonding of the type OH $\cdots$ N are known because of its versatility of their electronic and steric properties.<sup>26,27</sup> The imino group attracts great interest due to the existence of the intramolecular hydrogen bond between the -OH and the nitrogen atoms, which is similar to the case of benzimidazole phenolate.<sup>28,29</sup> There are different reports regarding the preparation of metal complexes with benzimidazole or Schiff base ligands due to their ability to stabilize such structures. Additionally, these compounds are applied in analytical chemistry for the heavy metals spectrophotometric determination.<sup>30,31</sup>

In this work, we describe the synthesis of new benzimidazole compounds with intramolecular H-bonding and the characterization of their chemical and biological properties. Hence, we report the synthesis of 2,4-di-tert-butyl-6-(3H-imidazo[4,5-c]pyridin-2-yl)phenol (**B2**), a compound derived from phenyl-3,5-di-tert-butyl-2-hydroxybenzoate (**B1**). Furthermore, we characterized **B2** by FTIR, <sup>1</sup>HNMR, HHCOSY, UV-vis, cyclic voltammetry, and luminescent properties assessed mainly by Quantum Yield and Life Time. We also compared **B2** and (E)-2-((3-amino-pyridin-3-ylimino)-methyl)-4,6-diterbutylphenol (**L2**), a Schiff base with antifungal properties reported by Carreño *et al.*<sup>32</sup> (see Scheme 1), with respect to the electrochemical, photophysical and antimicrobial properties. All the experimental results were supported and complemented with density functional (DFT) and time-dependent DFT (TDDFT) calculations.<sup>33-34</sup>



**Scheme 1.** Chemical structures of the compounds phenyl-3,5-di-tert-butyl-2-hydroxybenzoate (precursor, **B1**); 2,4-di-tert-butyl-6-(3H-imidazo[4,5-c]pyridine-2-yl)phenol (**B2**); 2,4-Di-tert-butyl-1-methoxy-benzene (compound with 2-methyl-3H-imidazo[4,5-c]pyridine) model (**B3**) used for the computational studies and (E)-2-[(3-aminopyridin-4-yl)imino]-methyl-4,6-di-tert-butylphenol (**L2**).

Regarding the biological properties, we assessed the antifungal activity of **B2** in the yeasts *Cryptococcus* spp., *Candida albicans*, *Candida tropicalis*, and in the mold *Botrytis cinerea*. *Cryptococcus* spp., and *Candida* species are opportunistic pathogens involved in potentially deadly diseases; whereas *Botrytis cinerea* is a phytopathogenic fungus infecting *ca.* 200 plant species causing the gray mold disease.<sup>35-36</sup> *Botrytis cinerea* is the main phytopathological problem that the fresh fruit export industry must deal with.<sup>37</sup> Control of *Botrytis* is performed by chemical fungicides implying various problems such as the emergence of resistant strains and environmental damage.<sup>38</sup> In this context, new fungicides based on modified benzimidazoles represent an alternative to control the gray mold diseased produced by *Botrytis*.<sup>40,41</sup> Besides fungi, we also tested the antimicrobial properties of **B2** against *Salmonella enterica* serovar Typhimurium (bacteria), an *Enterobacteriaceae* involved in the production of gastroenteritis in humans and systemic diseases in animals, such as mice.<sup>42,43</sup> We found that **B2** exerted antimicrobial activities against *Cryptococcus* spp. and *Botrytis cinerea*, unveiling a potential used as alternative antifungal agent.<sup>39</sup> Finally, due its particular fluorescence properties, we assessed the potential of **B2** to be used as a biological marker to observe bacteria, yeasts, and human

cells through confocal microscopy.

## 2. Experimental Section

**2.1 Synthesis.** All starting materials were purchased from Merck and Aldrich and used without further purification. The methods for preparations of the compounds are given below:

**Synthesis of the precursor phenyl-3,5-di-tert-butyl-2-hydroxybenzoate (B1).** The synthesis was prepared according to Benisvy *et al.*<sup>44,45</sup> The 3,5-di-tert-butyl-salicylic acid (20 mmol), N,N'-dicyclohexylcarbodiimide (28.8 mmol) and phenol (30 mmol) were added to dry THF (120 mL) and stirred for 4 days under nitrogen atmosphere at room temperature. The colorless oil was purified by column in pentane and recrystallized from chloroform. Suitable white crystal for X-rays was obtained with 38 % yield. <sup>1</sup>H NMR (400 MHz, CDCl<sub>3</sub>): δ= 1.51 [s, 9H, tBu]; 1.62 [s, 9H, tBu]; 7.36 [d, J=6.2 Hz; 2H], 7.44 [m; 1H], 7.59 [m; 2H], 7.81 [d; J=2.0 Hz; 1H]; 8.16 [d; J=2.4 Hz; 1H]; 11.33 [s; 1H].

**Synthesis of the 2,4-di-tert-butyl-6-(3H-imidazo[4,5-c]pyridine-2-yl)phenol (B2).** The synthesis was performed as previously described by Benisvy *et al.*<sup>44-46</sup> The phenyl-3,5-di-tert-butyl-2-hydroxybenzoate (1.87 mmol), 3,4-diaminopyridine (1.87 mmol) were added to nitrobenzene (30 mL) and refluxed with agitation for 4 h under nitrogen atmosphere as described.<sup>44</sup> The reaction mixture was evaporated to near dryness under high vacuum, to yield a dark brown oil, which was chromatographed, eluting first with hexane, and then with ethyl acetate. The fraction was evaporated, to give a brownish-yellow solid. The brown oil was purified by silica column in hexane/ethyl-acetate 1:15 (V/V). The product was recrystallized from ethanol. Yield 40%.

<sup>1</sup>H NMR (400 MHz, DMSO-d<sub>6</sub>): δ= 1.33 [s; 9H; tBu]; 1.43 [s; 9H; tBu]; 7.38 [d, J=1.9 Hz; 1H;H], 7.68 [d; J=4.7 Hz; 1H;H], 8.00 [s; 1H;H], 8.35 [d; J=5.3 Hz; 1H;H], 8.98 [s; 1H;H], 13.60 [s; 1H;O-H]. <sup>13</sup>C NMR (400 MHz, DMSO-d<sub>6</sub>): δ= 29.8; 31.7; 34.7; 121.8; 126.7; 136.8; 140.8; 155.9. UV/VIS: (Dichloromethane, room temperature, c= 3.45 x 10<sup>-6</sup> mol L<sup>-1</sup>) λ(ε)= 229 (24800 mol<sup>-1</sup> dm<sup>3</sup> cm<sup>-1</sup>), 302 (18491 mol<sup>-1</sup> dm<sup>3</sup> cm<sup>-1</sup>), 356 (11758 mol<sup>-1</sup> dm<sup>3</sup> cm<sup>-1</sup>). (Ethanol, room temperature, c= 3.45 x 10<sup>-6</sup> mol L<sup>-1</sup>) λ(ε) = 220 (38184 mol<sup>-1</sup> dm<sup>3</sup> cm<sup>-1</sup>), 293 (19147 mol<sup>-1</sup> dm<sup>3</sup> cm<sup>-1</sup>), 330 (11725 mol<sup>-1</sup> dm<sup>3</sup> cm<sup>-1</sup>). FTIR (cm<sup>-1</sup>): 3440 (νOH); 1627 (νCN); 1590 (νCC). EI-MS 323 M<sup>+</sup>.

## 2.2 Characterization

UV-Vis and fluorescence spectra were performed using a UV-Vis-NIR scanning spectrophotometer Shimadzu Model UV-3101 PC, and Perkin Elmer LS55 Luminescence Spectrometer. The NMR spectra were recorded on a Bruker AVANCE 400 spectrometer at 25 °C. Samples were dissolved in deuterated acetonitrile, using tetramethylsilane as an internal reference. IR spectra were obtained on a Perkin-Elmer 1310 or in a Bruker Vector-22 FT-IR spectrophotometer, in KBr discs. UV-vis spectra were performed using a Shimadzu Model UV-3101 PC UV-vis-NIR scanning spectrophotometer. Steady-state photoluminescence (PL) spectra were measured on an ISS K2 fluorimeter. Samples in CH<sub>3</sub>CN were sparged with argon for 30 minutes and excited at  $\lambda \approx 355$  nm. The intensity was integrated for 0.5 seconds at 2 nm resolution. PL quantum yields were measured through comparative actinometry using [Ru(bpy)<sub>3</sub>] [PF<sub>6</sub>]<sub>2</sub> in acetonitrile ( $\phi_{em} = 0.062$ ) as a quantum yield standard.<sup>47,48</sup> Time-resolved PL decays using a tripled ND:YAG laser at 355 nm excitation. The doubled ND:YAG (532 nm) was passed through a Raman tube pressurized with H<sub>2</sub>.

For the electrochemical experiments, the working solution contained  $1.0 \times 10^{-2}$  mol·L<sup>-1</sup> of **B2** compound with  $1.0 \times 10^{-1}$  mol·L<sup>-1</sup> of tetrabutylammonium hexafluorophosphate (TBAPF<sub>6</sub>) as supporting electrolyte in anhydrous acetonitrile (ACN). Prior to each experiment, the solution was purged with high purity argon, and an argon atmosphere was maintained over the solution during the whole experiment. A polycrystalline non-annealed platinum disc (diameter 2 mm) was used as working electrode. As counter electrode, platinum gauze of large geometrical area was employed, separated from the cell main compartment by a fine grain sintered glass. All potentials quoted in this text refer to an Ag|AgCl electrode in tetramethylammonium chloride to match the potential of a saturated calomel electrode (SCE) at room temperature. All electrochemical experiments were performed at room temperature on a CHI900B bipotentiostat interfaced to a PC running the CHI 9.12 software that allowed experimental control and data acquisition.

### 2.3 Preliminary quenching fluorescence study

Stock solutions of 2,4-di-tert-butyl-6-(3H-imidazo[4,5-c]pyridine-2-yl)phenol in ethanol ( $2.84 \times 10^{-5}$  M) or acetonitrile ( $4.7 \times 10^{-5}$  mol L<sup>-1</sup>) were used. Also, stock solution of the hydrated salts Hg(NO<sub>3</sub>)<sub>2</sub>\*H<sub>2</sub>O ( $9.19 \times 10^{-4}$  mol L<sup>-1</sup>) was prepared in distilled water at pH 6.0. Test solutions were prepared by placing 3 mL of **B2** solution in ethanol or acetonitrile into quartz cuvettes, adding aliquot of aqueous Hg<sup>2+</sup>. Fluorescence spectra were obtained using a Perkin Elmer LS55 Luminescence Spectrometer. Both the excitation and emission slit widths were 5.0 nm.

### 2.4 Computational details

All structural and electronic properties of **B2** were obtained using the Amsterdam Density Functional (ADF) code.<sup>49</sup> The molecular structures were fully optimized by an analytical energy gradient method as implemented by Verluis and Ziegler,<sup>50</sup> using the hybrid B3LYP functional<sup>51</sup> and the standard Slater-type-orbital (STO) basis set with triple- $\zeta$  quality double plus polarization functions (TZ2P) for all the atoms.<sup>52</sup> Frequency analyses were performed after the geometry optimization to corroborate the minimum and to compare with experimental infrared (FTIR) spectra. Additionally, to evaluate the importance of the hydrogen bond, we propose a second model replacing the -OH group with a -OCH<sub>3</sub> (methoxy) group and reoptimized the new structure B3 model (**Schema 1**). The same analysis for **B2** was performed on the new structure to elucidate the role of the intramolecular hydrogen bond. Time-dependent density functional theory (TDDFT)<sup>52</sup> was used at the same level of calculation to model the excitation energies using in all cases the conductor-like screening model (COSMO)<sup>53</sup> for a realistic modeling of solvent effects. Three different media with distinct polarity were considered in the calculation: acetonitrile, ethanol and dichloromethane to estimate the hydrogen bond stability. In addition, the calculations were also performed in the gas phase.

In particular, **B2** also presented an emission band around 500 nm and it was possible to model this emission using TDDFT. The first step in the calculations was a regular optimization of the excited state. After that, we performed again a TDDFT calculation using the optimized geometry. At this level, it was possible to associate the calculated absorption energies with the molecular emission. More detailed calculations were performed by using the self-consistent two-component spin-orbit coupling

TDDFT (SOC-TDDFT) within the ZORA Hamiltonian, even when in organic compounds the spin-orbit coupling have not a large contribution. In ADF, this kind of calculation allowed us to better estimate the emission wavelength. In all cases, at least five spin-mixed excitations were calculated in the full SOC-TDDFT calculations. The GGA SAOP (statistical average of orbitals exchange correlation potential) functional, specially designed for the calculations of optical properties, was used.<sup>54</sup> Environmental effects were included via COSMO continuum solvation model using acetonitrile parameters.

## 2.5 Antimicrobial Activity

All the compounds were evaluated for their *in vitro* growth inhibitory activity against a Gram-negative pathogen *Salmonella enterica* serovar Typhimurium ATCC14028s (*S. enterica*), and the clinical yeasts *Candida albicans*, *Candida tropicalis* and *Cryptococcus* spp. obtained from the Hospital Clínico of the Universidad de Chile, Santiago, Chile. Minimum inhibitory concentration (MIC) was obtained by broth dilution. The MIC is defined as the lowest concentration of the tested compounds at which no growth of the strain was observed after the incubation. *S. enterica* was previously grown in Luria-Bertani broth (Bacto peptone, 10 g/l; Bacto yeast extract, 5 g/l; NaCl, 5 g/l) at 37 °C with shaking to OD<sub>600</sub> = 1.4 (stationary phase). Yeasts were previously cultured in Sabouraud agar (Bacto peptone, 10 g/L; glucose, 40 g/L; agar, 15 g/L; pH 5.6) at 28 °C. Further dilutions of microorganisms (bacteria and yeasts; 0.5 McFarland) were performed with Bacto Tryptic Soy broth (pancreatic digest casein 17.0 g/l, papaic digest of soybean 3.0 g/l, dextrose 2.5 g/l, sodium chloride 5.0 g/l, dipotassium phosphate 2.5 g/l). Stock solutions of the tested compounds were prepared in dimethyl sulfoxide (DMSO) for **L2**, **B2**, ketoconazole (**K1**, control), and fluconazole (**K2**, control); or in ethanol 95% for chloramphenicol (**C1**, control). The concentration range of the compounds tested was between 0.10 ppm and 200 ppm. The inoculated wells were incubated at 37 °C for 24 h (bacteria), or at 28 °C for 48 h (yeasts). A control, DMSO and ethanol 95% without any tested compound, were included when necessary. Only when the inhibition effects of the tested compounds were distinguishable from DMSO alone (in the case of **L2**, **B2**, **K1**, and **K2**), or from ethanol 95% alone (in the case of **C1**), the compound was considered to exhibit antimicrobial activity. The MIC values of the tested compounds were obtained as ppm. All the experiments were performed in triplicate. To qualitatively determine the antifungal activity of **L2**, **B2**, and DMSO (vehicle, control), a standard disk diffusion assay was used, with the following

modifications. Overnight cultures of *Cryptococcus* spp., *Candida albicans* and *Candida tropicalis* were suitable diluted to seed approximately  $10^6$  cfu in a Sabouraud plate. Then, two metal rings were put on the plate prior to being filled with 100  $\mu$ l of **L2** (400 ppm), 100  $\mu$ l of **B2** (400 ppm), or 100  $\mu$ l of DMSO alone (control). When the agar plate absorbed the compounds, the metal rings were removed. Yeasts were incubated 48 h at 28 °C prior to determining the inhibition zone diameters, obtained as the average of two measurements along two axes passing through the center of the disk by duplicate. In all cases, diameters differed by no more than 1 mm.

*Botrytis cinerea* strain B05.10 was used in all the experiments. To evaluate the effect of **B2** and **L2** on the growth of this strain, a stock solution of compound **B2** and **L2** were prepared in DMSO. Potato dextrose agar (PDA) plates were prepared containing compound **B2** or **L2** in the range of 2 to 10 ppm. Subsequently, a disk of APD with actively growing fungus was deposited in the center of the plate and it was incubated at 4 °C during 9 days. The radial growth of the fungus on each plate was measured until the control plate (no compound, only DMSO) reached its maximum growth. As control of fungicide activity, we used the commercial product fenhexamid, at a dose of 2 ppm. Two biological and three technical replicates were performed to each experiment. The average values of the diameter growth were plotted and statistically analyzed using ANOVA and Tukey test.

## 2.6 Bacteria uptake studies

To determine the correlation between bacterial concentration and **B2**-dependent fluorescence, we performed the following procedure. Bacteria were grown in LB to  $OD_{600} = 1.4$  (stationary phase) prior to being washed twice and being resuspended in one volume of phosphate buffer solution (PBS). Then, bacteria were serially diluted with PBS and each dilution was mixed with one volume of **B2** (100 ppm in DMSO). The mixtures were incubated 5 min at 37 °C and subsequently centrifuged approximately at 20 000  $xg$  for 3 min to separate the pellets and supernatants. Fluorescence in each supernatant fraction was measured using RF-5301 PC spectrofluorophotometer Shimadzu with Xe lamp (excitation: 350 nm; detection: 500 nm) in a cuvette with 2 mL of dichloroethane and 10  $\mu$ L of sample. The pellets were washed 4 times with PBS to remove any unattached **B2**. Finally, the fraction of **B2** attached to bacteria was recovered by resuspending the pellets in DMSO prior to centrifuging approximately at 20 000  $xg$  for 3 min to discard the pellet. Fluorescence, corresponding to the **B2** attached to bacteria, was measured following the same procedure described above. The experiments were performed in

duplicate.

## 2.7 Fluorescence studies and confocal microscopy

*Salmonella enterica* serovar Typhimurium ATCC14028s (*S. enterica*) or *Escherichia coli* DH5 $\alpha$  / pGLO<sup>mut</sup> (GFP<sup>+</sup>) were grown in Luria-Bertani broth to OD<sub>600</sub> = 1.4 (stationary phase). pGLO<sup>mut</sup> plasmid (simply called pGLO in this paper) harbors GFP under a promoter exhibiting a spontaneous mutation that produces GFP constitutively without the need of arabinose as inducer (unpublished results). *Candida albicans* was grown in Sabouraud agar at 28 °C. Bacteria or yeasts were washed twice with phosphate buffer solution (PBS) prior to add one volume of 400 ppm **B2** and incubate 5 min at 37 °C. To remove the excess of **B2**, microorganism was washed four times with PBS, to finally be resuspended in PBS. All the samples were observed fresh to determine localization of **B2** by confocal microscopy. Human ovarian adenocarcinoma cell line (SKOV-3) was grown in Dulbecco's Modified Eagle's Medium (DMEM) supplemented with 10% v/v fetal bovine serum and 1% penicillin-streptomycin solution (HyClone™, South Logan, Utah, USA). Cells were incubated at 37°C and 5% CO<sub>2</sub>. Cells were seeded on 24-well plates in coverslips and incubated for 24 h. Then, cells were washed twice with PBS and cells were incubated with **B2** solution (400 ppm) for 15 min. After incubation time, cells were washed with PBS and fixed for 10 min with 4% paraformaldehyde followed by washes with PBS. Finally, cells were mounted on glass slides using Fluoromount-G (Electron Microscopy Sciences, Hatfield, Pennsylvania, USA). Detection of the **B2** or GFP was performed using a FV1000 laser scanning confocal microscope (Olympus, USA). Bacteria, yeasts, or human cells were treated as described above before the observation. Fluorescence emission was obtained by laser excitation of **B2** at 405 nm, and GFP at 488. Emission was collected with a long-pass emission filter in the range of 425 nm to 525 nm for **B2**, and 500 nm to 600 nm for GFP. Since we observed that yeasts presented autofluorescence, as assessed by confocal microscopy, we set detection threshold using yeasts treated with DMSO alone.

### 3. Results and Discussion

#### 3.1 Synthesis and characterization

Precursor phenyl-3,5-di-*tert*-butyl-2-hydroxybenzoate (**B1**) was obtained as a white solid with 38% yield. The synthesis of 2,4-di-*tert*-butyl-6-(3H-imidazo[4,5-*c*]pyridine-2-yl)phenol (**B2**) was accomplished by condensation of 3,4-diaminopyridine and phenyl 3,5-di-*tert*-butyl-2-hydroxybenzoate in nitrobenzene, using a slight modification of the method reported by Benisvy *et al.*<sup>44</sup> for the analogous phenyl-3,5-di-*tert*-butyl-2-hydroxybenzoate (Yield 40%).

The FT-IR spectra of compound **B2** absorption frequencies showed strong symmetric and asymmetric narrow bands due to O-H vibrations at 3440 cm<sup>-1</sup>. Other absorption frequencies were observed at 1627 and 1590 cm<sup>-1</sup>, assigned to C=N and C=C stretching, respectively.<sup>55,56</sup> The <sup>1</sup>H NMR spectra (in CDCl<sub>3</sub>) for **B1** showed an intramolecular hydrogen bond signal at 11.33 ppm according to literature.<sup>57</sup> For **B2**, 1D and 2D NMR spectra were obtained in DMSO-*d*<sub>6</sub> solutions (Proton numbering, Scheme, and <sup>1</sup>H NMR spectra are given in Figures S1- S2, ESI<sup>†</sup>). The <sup>1</sup>H NMR spectrum exhibited a strong narrow signal at approximately 13.6 ppm (See figure S3, ESI<sup>†</sup>) for -OH evidence of the strong intramolecular hydrogen bond character, analogous to the intramolecular hydrogen bond described for **L2**.<sup>32</sup> After D<sub>2</sub>O exchange, these signals disappeared from the spectrum (data not show). The signals assigned to the *tert*-butyl groups appeared at 1.47 and 1.28 ppm and the aromatic protons of both rings appeared at 7.50 - 6.70 ppm and 8.60 - 8.00 ppm, respectively. 2D NMR spectra was recorded for the assignment of aromatic protons (Figure S4, ESI<sup>†</sup>). The pyridine H2, H3 and H1 protons appeared at 6.72, 7.24 and 8.01 ppm, respectively. A signal assigned to the benzimidazole carbon atom (Figures S5-S6, ESI<sup>†</sup>) was observed approximately at 156 ppm for **B2**. The ESI mass spectrum of **B2** (see Figure S7, ESI<sup>†</sup>) showed a major fragment at *m/z* = 323, in agreement with the expected value for the molecular ion.

To understand the electronic structures of 2,4-di-*tert*-butyl-6-(3H-imidazo[4,5-*c*]pyridine-2-yl)phenol (**B2**), compared with (*E*)-2-[(3-aminopyridin-4-yl)imino]-methyl-4,6-di-*tert*-butyl-phenol (**L2**),<sup>32</sup> we performed DFT calculations using the approaches explained above. The first step in the calculations was a geometry optimization of the neutral compound **B2**. The oxidized and reduced forms were also calculated and compared with the neutral form. The geometrical parameters in the three structures were similar without significant differences. The most important atom distances are in good agreement with

the experimental crystallographic data reported for similar compounds in our previous publication.<sup>32</sup> Unfortunately, the X-Ray crystal data for **B2** is not reported, but due to the similarities with **L2** we concluded that the geometrical differences for –CH=N- and C-O moieties distances were negligible. However, a significant difference was observed in the intramolecular hydrogen bond and O-H distances, due the planar (closed ring) structure in **B2** in comparison with **L2**.<sup>32</sup>

**B2** and **L2** showed an intramolecular hydrogen bond distance OH...N of 1.695 (Figure 1) and 1.582 Å<sup>32</sup>, respectively. All calculated distances for **B2** and **L2** are summarized in Table 1.

Also the strength of the hydrogen bond was estimated for **B2** by comparing the energy of the molecule with a conformer where the hydrogen bond was broken. The energy difference was 22.0 Kcal/mol which is an evidence of the importance of this interaction in the stabilization of the molecule. This was corroborated from the H-NMR discussed above.

The cationic or anionic form of **B2** and **L2** maintain the same conformation of the neutral form due to the intramolecular hydrogen bond,<sup>45,46</sup> with an increment in the -HC=N- distance for **L2** charged forms,<sup>32</sup>. In the same way, the calculated frequencies for **B2** are in good agreement with the values observed in the FT-IR spectra for the most important functional groups in similar compounds.<sup>58</sup> All the frequencies were positive, meaning that the most stable conformation was determined.

The main functional groups of both compounds appears in the same region of the spectra with some differences due to the different conformation of the molecules (see Table 2), the frequencies are in good agreement with our previous reported work for **L2**.<sup>32</sup>

**Table 1.** Geometrical parameters calculated for 2,4-di-ter-butyl-6-(3H-imidazo[4,5-c]pyridine-2-yl)phenol (**B2**) and (*E*)-2-{[(3-aminopyridin-4-yl)imino]-methyl}-4,6-di-tert-butyl-phenol (**L2**)<sup>32</sup> in neutral, oxidized and reduced forms. All distances are in Å.

Molecule	d(N-H) H bond	d(O-H)	d(C=N)	d(C-NH)	d(C-O)
<b>B2</b>	1.695	0.990	1.318	1.378	1.345
<b>B2</b> <sup>+</sup>	1.695	0.991	1.318	1.378	1.345
<b>B2</b> <sup>-</sup>	1.695	0.991	1.317	1.378	1.345
<b>L2</b>	1.582	1.034	1.301	1.380	1.356
<b>L2</b> <sup>+</sup>	1.534	1.053	1.317	1.344	1.325
<b>L2</b> <sup>-</sup>	1.501	1.065	1.365	1.399	1.374

Abbreviations: **B2**<sup>+</sup> = cationic; **B2**<sup>-</sup> = anionic.

**Table 2.** Calculated vibrational frequencies (in cm<sup>-1</sup>) for the main groups of 2,4-di-ter-butyl-6-(3H-imidazo[4,5-c]pyridine-2-yl)phenol (**B2**) and (*E*)-2-{[(3-aminopyridin-4-yl)imino]-methyl}-4,6-di-tert-butyl-phenol (**L2**)<sup>32</sup>.

IR-SPECTRUM	$\nu_s(\text{C-NH})$	$\nu(\text{OH})$	$\nu(-\text{C=N-})$
<b>B2</b>	3685	3251	1556-1661
<b>L2</b>	3458	3350	1562-1582

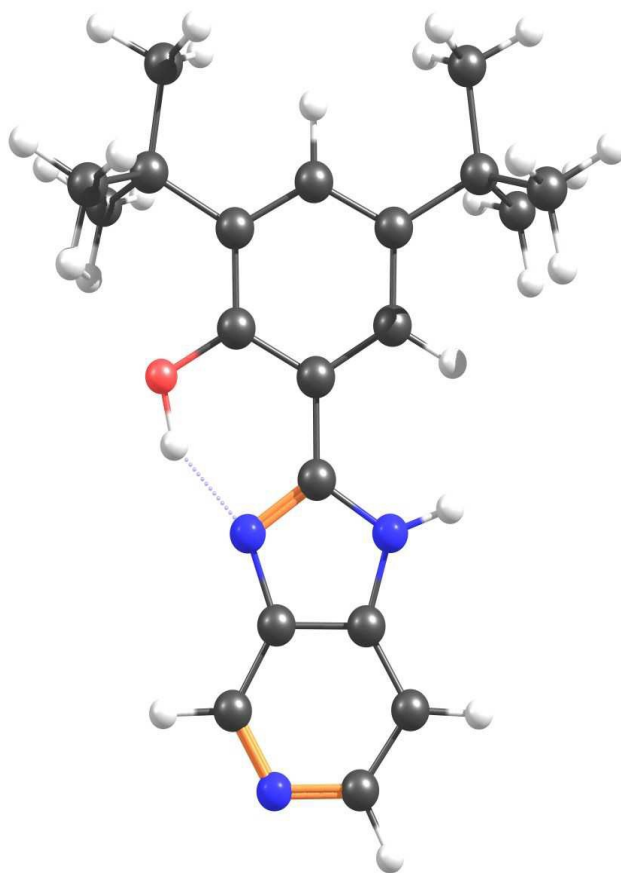


**Figure 1.** DFT optimized structure of 2,4-di-ter-butyl-6-(3H-imidazo[4,5-c]pyridine-2-yl)phenol (**B2**).

The absorption and emission spectra of **B2** in dichloromethane and ethanol were recorded at room temperature (Figures S8-S11, ESI†). It can be observed that the **B2** spectrum had three intense absorption bands at 229 nm ( $\epsilon=2.5 \times 10^4 \text{ dm}^3 \text{ mol}^{-1} \text{ cm}^{-1}$ );  $\lambda_{\text{max}}=302 \text{ nm}$  ( $\epsilon=1.8 \times 10^4 \text{ dm}^3 \text{ mol}^{-1} \text{ cm}^{-1}$ ) and at  $\lambda_{\text{max}}=356 \text{ nm}$  ( $\epsilon=1.2 \times 10^4 \text{ dm}^3 \text{ mol}^{-1} \text{ cm}^{-1}$ ) in dichloromethane. In ethanol, these bands appeared at 220 nm ( $\epsilon=3.8 \times 10^4 \text{ dm}^3 \text{ mol}^{-1} \text{ cm}^{-1}$ );  $\lambda_{\text{max}}=293 \text{ nm}$  ( $\epsilon=1.9 \times 10^4 \text{ dm}^3 \text{ mol}^{-1} \text{ cm}^{-1}$ ) and at  $\lambda_{\text{max}}=330 \text{ nm}$  ( $\epsilon=1.2 \times 10^4 \text{ dm}^3 \text{ mol}^{-1} \text{ cm}^{-1}$ ), respectively. The first one corresponded to the  $n \rightarrow \pi^*$  transition, while the second and third were usually assigned to two different  $\pi \rightarrow \pi^*$  by analogy with similar organic compounds.<sup>59,60</sup>

The UV-vis absorption and emission (excited at  $\lambda \approx 355$  nm) spectra for **B2** obtained at room-temperature, were taken in acetonitrile under argon atmosphere (Figure S12, ESI<sup>†</sup>). **B2** showed a broad emission band, with a maximum approximately at 500 nm. A large Stoke shift could be observed, suggesting an important structural change between the ground and excited states. The lifetimes were faster than the instrument response, suggesting a fluorescence emission character.

**Table 3:** Photophysical properties of 2,4-di-*tert*-butyl-6-(3H-imidazo[4,5-c]pyridine-2-yl)phenol (**B2**).

Compound	T (ns)	QY	$k_r$ ( $M^{-1} s^{-1}$ )	$k_{nr}$ ( $M^{-1} s^{-1}$ )
<b>B2</b>	$< 10^a$	0.21	$2.1 \times 10^7{}^c$	$7.9 \times 10^7{}^d$

<sup>a</sup>Lifetimes were faster than the instrument response. <sup>c,d</sup>These values are an approximated upper limit.

Time dependent density functional theory (TD-DFT) calculations were conducted to further elucidate the UV-vis transitions in three different solvents and in gas phase (see Figure 3 (A) and S13, ESI<sup>†</sup>). The UV-vis calculated spectra in dichloromethane, ethanol and acetonitrile showed absorption bands centered at 200 nm and 375 nm (see Table 4) for **B2**, which were assigned to  $n \rightarrow \pi^*$  (C=N) and  $\pi \rightarrow \pi^*$  transitions, respectively. The calculated transitions showed that excitations associated to  $n \rightarrow \pi^*$  (C=N) in the benzimidazole had a composition of HOMO-5  $\rightarrow$  LUMO in acetonitrile, and HOMO-4  $\rightarrow$  LUMO for ethanol, dichloromethane and gas phase. The bands assigned as  $\pi \rightarrow \pi^*$  transitions involved compositions of HOMO-1  $\rightarrow$  LUMO and HOMO  $\rightarrow$  LUMO in all the solvents and in gas phase. The comparison between the solvent spectra with the gas phase showed no significant shift in the UV-vis spectra when the solvent polarity changed, confirming the stability of the intramolecular hydrogen bond.<sup>61</sup>

From the MO diagram of **B2** (Figure 2) and **L2**<sup>32</sup>, it is possible to see that both compounds share some electronic similarities and differences around their frontier orbitals, affecting their electrochemical and optical properties. The HOMO in **B2** is located at the phenolic ring while for **L2** HOMO-1 is found on this moiety. However, the HOMO in **L2** corresponded to a molecular orbital mainly located at the pyridine ring. On the other hand, the LUMO in **B2** and **L2** are distributed along the phenolic and pyridine ring with some minor differences between them. Also, the HOMO-LUMO gap showed a difference of 2.75 eV for **L2** and 3.07 eV for **B2**. Figure 2 showed qualitatively molecular orbital diagram for 2,4-di-*ter*-butyl-6-(3H-imidazo[4,5-c]pyridine-2-yl)-phenol (**B2**) with the most important

electronic transitions (For **L2** see reference 32). From these differences between the HOMOs, arise the electrochemical differences, related with the stabilization of the phenoxy radical when one electron is removed from both systems.<sup>21-23</sup> and discussed in the electrochemical studies as below.

**Table 4.** Maximum absorption wavelengths (nm), molar extinction coefficients ( $10^{-3} \text{ mol}^{-1} \text{ dm}^3$ ) (determined experimentally), and maximum absorption wavelengths (nm), energy (eV) and nature of the electronic transitions (determined by calculations) for 2,4-di-ter-butyl-6-(3H-imidazo[4,5-c]pyridine-2-yl)phenol (**B2**).

	$\lambda_{\text{exp}}$	$\epsilon$	$\lambda_{\text{cal}}$	$f (\times 10^{-1})$	Assignment
<b>Dichloromethane</b>	229	24.8	224	0.016	HOMO-5 $\rightarrow$ LUMO $n \rightarrow \pi^*$
	302	18.4	303	4.0	HOMO-1 $\rightarrow$ LUMO $\pi \rightarrow \pi^*$
	356	11.7	361	1.3	HOMO $\rightarrow$ LUMO $\pi \rightarrow \pi^*$
<b>Ethanol</b>	220	38.1	236	0.076	HOMO-4 $\rightarrow$ LUMO $n \rightarrow \pi^*$
	293	19.1	307	8.1	HOMO-1 $\rightarrow$ LUMO $\pi \rightarrow \pi^*$
	330	11.7	362	3.2	HOMO $\rightarrow$ LUMO $\pi \rightarrow \pi^*$
<b>Acetonitrile</b>	---	---	228	0.054	HOMO-4 $\rightarrow$ LUMO $n \rightarrow \pi^*$
	---	---	318	8.2	HOMO-1 $\rightarrow$ LUMO $\pi \rightarrow \pi^*$
	---	---	370	3.2	HOMO $\rightarrow$ LUMO $\pi \rightarrow \pi^*$
<b>Gas</b>	---	---	201	0.027	HOMO-4 $\rightarrow$ LUMO $n \rightarrow \pi^*$
	---	---	301	3.5	HOMO-1 $\rightarrow$ LUMO $\pi \rightarrow \pi^*$
	---	---	369	1.1	HOMO $\rightarrow$ LUMO $\pi \rightarrow \pi^*$

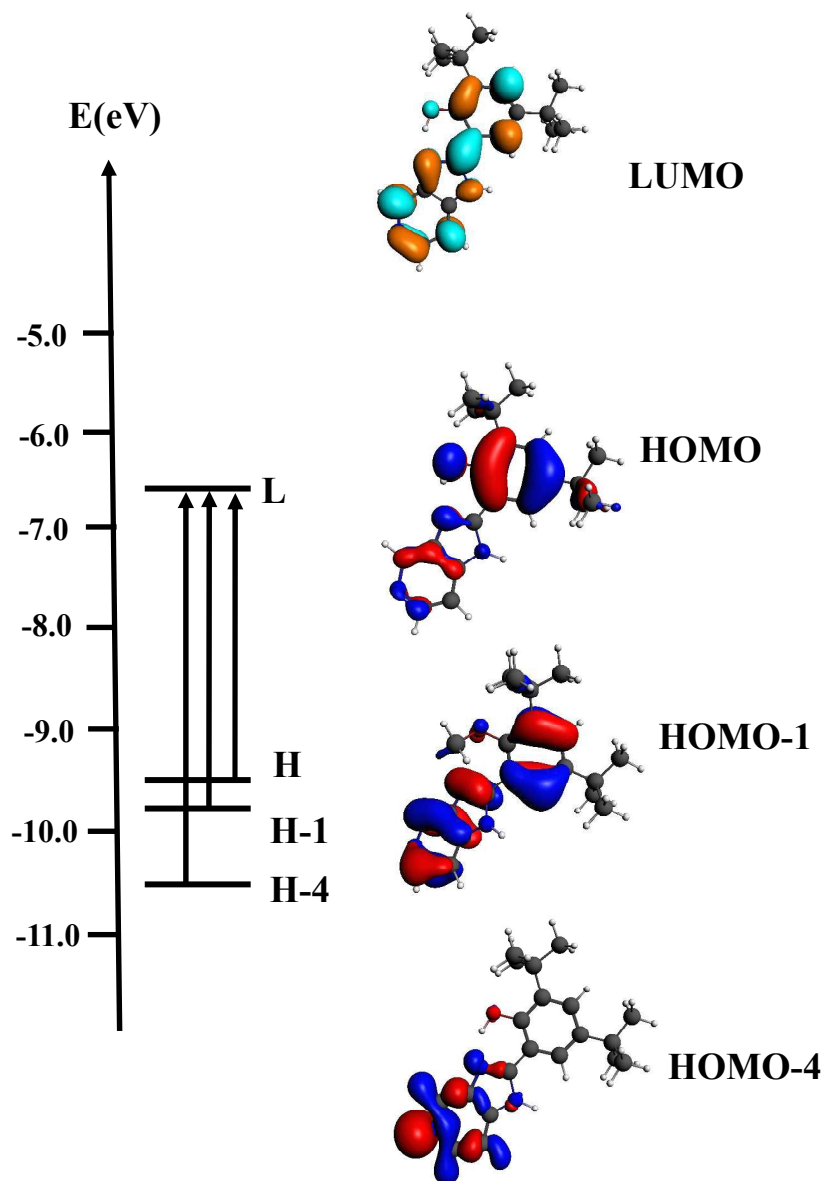


**Figure 2.** Qualitatively Molecular Orbital diagram for 2,4-di-ter-butyl-6-(3H-imidazo[4,5-c]pyridine-2-yl)-phenol (**B2**) with the most important electronic transitions.

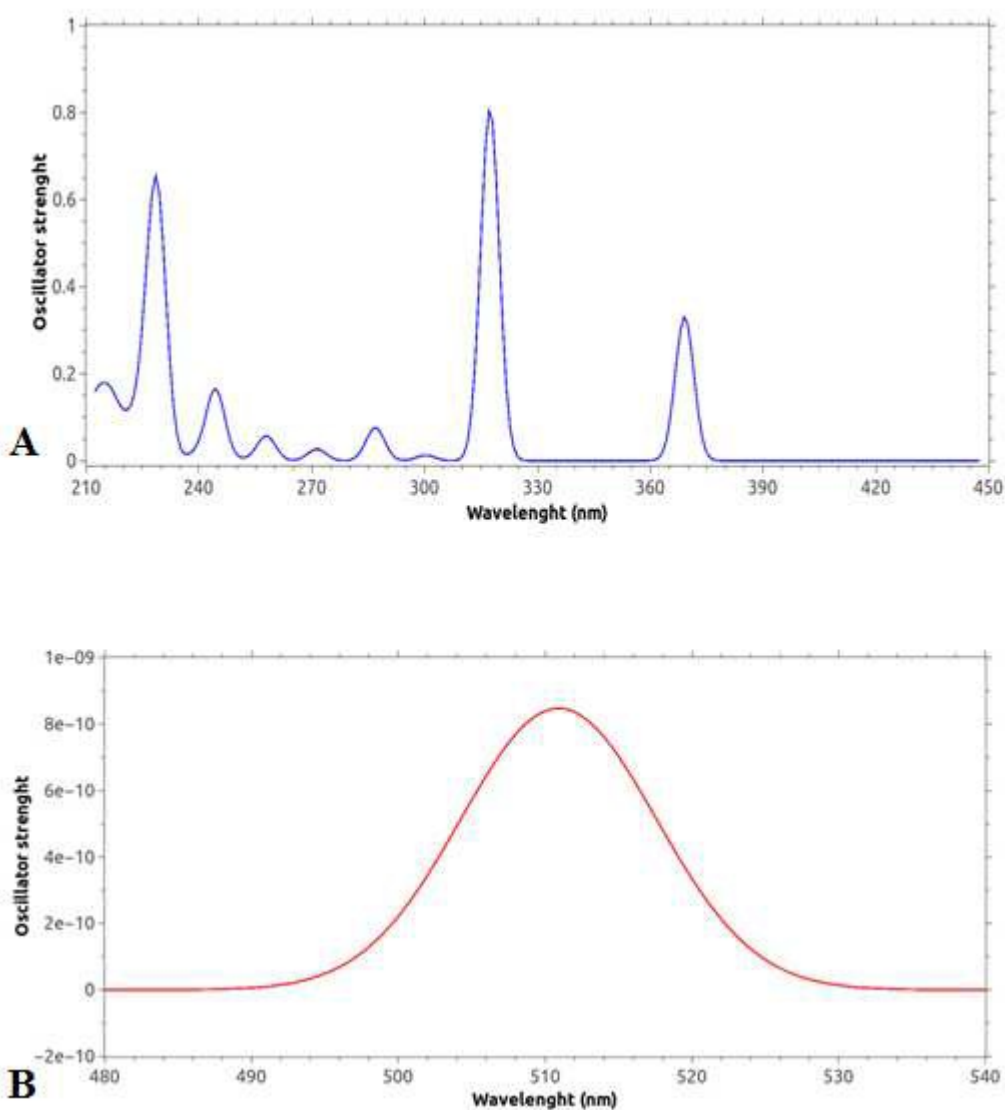


**Figure 3.** Calculated UV-vis absorption (A) and emission (B) spectra for 2,4-di-ter-butyl-6-(3H-imidazo[4,5-c]pyridine-2-yl)phenol (**B2**) in acetonitrile solvent.

On the other hand, the calculation of the emission spectra of **B2**, Figure 3 (B), is in agreement with the experimental data showing an emission around 510 nm in acetonitrile solvent. **B2** exhibited luminescent properties, contrary to **L2**.<sup>32</sup> These results show that the emission of **B2** is a consequence of the rigidity of the structure which substantially reduce the vibronic relaxation due the strong

intramolecular hydrogen bond.<sup>62,63</sup> In the case of **L2**, the excited state loss its rigidity and the probability of emission was reduced because of a break in the conjugation between both rings, with the consequent increment of the dihedral angle between the rings.<sup>64,65</sup> To assess the role of the intramolecular hydrogen bond, we broke this interaction by replacing the -OH groups by -OCH<sub>3</sub> (**B3** model). We observed in **B3** an increase of 42° in the dihedral angle between rings. When the hydrogen bond was eliminated, the following distances were found: 1.375, 1.327 and 1.386 Å for C-OCH<sub>3</sub>, -C=N-, and C-NH, respectively. These changes were a consequence of the torsion between the two rings in the molecular model (see Figure 4). Unfortunately, it was impossible to make a methylation of the hydroxyl groups in **B2** when we treated with diazomethane reactions,<sup>66</sup> supporting the great stability of the intramolecular hydrogen bond and its major contribution to **B2** geometry and properties. We observed the same results with **L2** (data not shown).

**Table 5.** Maximum absorption wavelengths (nm) determined by calculations, and nature of the electronic transitions for 2,4-Di-tert-butyl-1-methoxy-benzene (compound with 2-methyl-3H-imidazo[4,5-c]pyridine) model (**B3**).

	$\lambda_{\text{cal}}$	$f (x10^{-1})$	Assignment
<b>Acetonitrile</b>	240	0.14	HOMO-3-LUMO $n \rightarrow \pi^*$
	313	2.1	HOMO-1-LUMO $\pi \rightarrow \pi^*$
	351	7.8	HOMO-LUMO $\pi \rightarrow \pi^*$

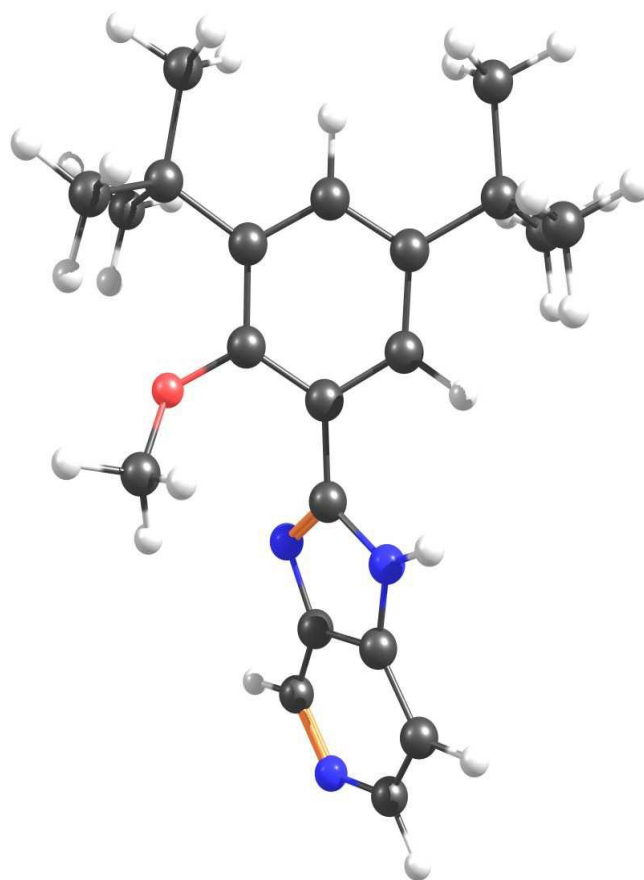


**Figure 4.** DFT optimized structure of 2,4-Di-tert-butyl-1-methoxy-benzene (compound with 2-methyl-3H-imidazo[4,5-c]pyridine) model (**B3**).

### 3.2 Electrochemical studies.

The electrochemical study of 2,4-di-*tert*-butyl-6-(3H-imidazo[4,5-*c*]pyridine-2-yl)-phenol (**B2**) consisted essentially on cyclic voltammetry experiments (Figure 5) in solutions containing the analyte (straight lines) compared against the same experiment done in solution with supporting electrolyte only (dashed lines). The electrochemical study of (*E*)-2-[[3-(aminopyridin-4-yl)imino]-methyl]-4,6-di-*tert*-butyl-phenol (**L2**) was previously reported by Carreño *et al.*<sup>32</sup>

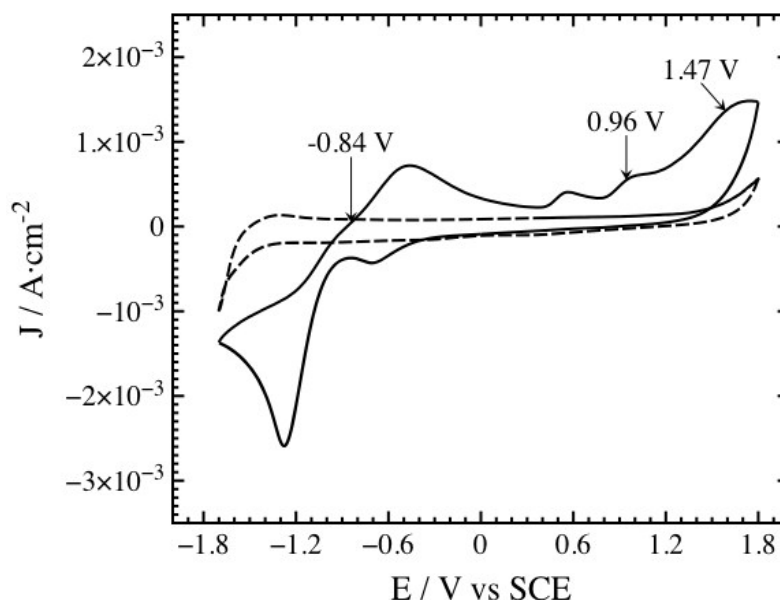


**Figure 5.** CV profiles of compound 2,4-di-*tert*-butyl-6-(3H-imidazo[4,5-*c*]pyridine-2-yl)phenol (**B2**). Interface: Pt | 0.01 mol L<sup>-1</sup> of compound + 0.1 mol L<sup>-1</sup> of TBAPF<sub>6</sub> in anhydrous CH<sub>3</sub>CN under an argon atmosphere. Scan rate: 200 mV s<sup>-1</sup>.

At first glance, several signals were observed for **B2**. Irreversible oxidation processes at potential peak ( $E_p$ ) +0.96 and +1.47 V, were identified. Furthermore, towards the cathodic potential limit, an important quasireversible reduction process at a half wave potential ( $E_{1/2}$ ) of -0.84 V could be observed. This peak description could be better understood by checking the working window displayed in Figure 6. Different potential ranges were used to check the dependence of each signal with the others and their reversibility character.

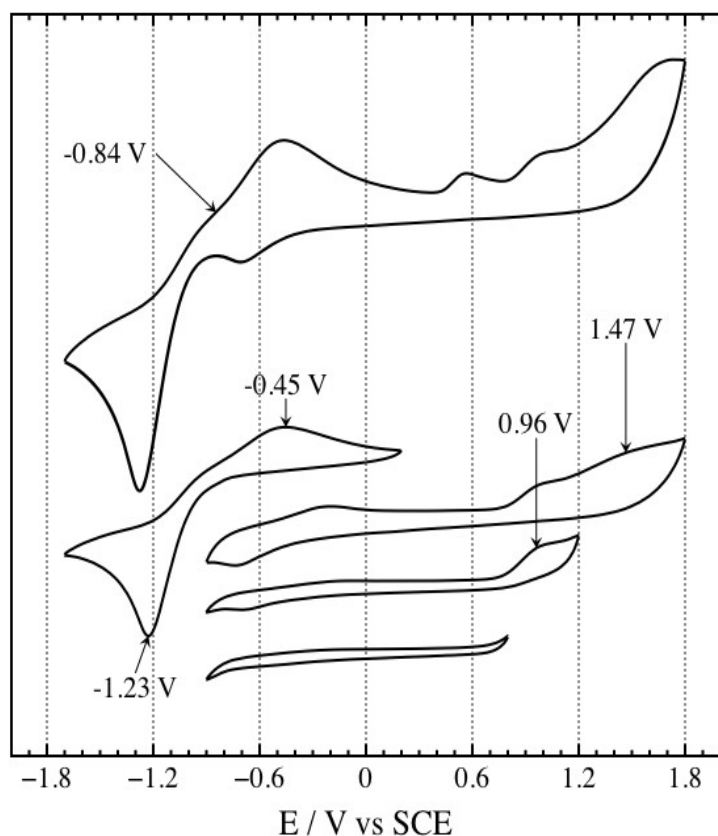


**Figure 6.** CV working-window study of 2,4-di-tert-butyl-6-(3H-imidazo[4,5-c]pyridine-2-yl)phenol (**B2**). Interface: same as Fig. 5.

As shown in Figure 6 (from bottom to top), the signals appeared showing their nature. The first profile proved that scanning between -0.90 and +0.80 V did not induce any red-ox processes. As the potential window widens **B2** exhibited a quasireversible reduction process at  $E_{1/2} = -0.84$  V vs SCE. Such quasireversible character stabilization is attributed to proton transfer from the phenol moiety to the bulk of the solution.<sup>63,64</sup> In other words, the isomazole moiety induces a strong cathodic response due to a quasireversible process, with reduction and oxidation processes at -1.28 and -0.47 V vs SCE, respectively. These processes were determined as dependent one from the other, attributable to the stabilization of an electron of the oxidation product due to the proton transfer at the O-H $\cdots$ N moiety. Towards the anodic potential limit, two independent irreversible oxidation peaks at +0.96 and +1.47 V vs ECS are evident (Figure 6). **L2** also presented two irreversible oxidation processes<sup>32</sup> ( $E_p = +0.71$  and +1.35 V vs ECS, respectively) assigned to oxidation of -NH<sub>2</sub> and -OH groups.<sup>65,66</sup> Since reproducibility of the methods used and the similar structure of the molecules, these same designations

may be attributed to the oxidation processes seen in **B2**.<sup>21-23</sup> The difference between the  $E_p$  values both compound may be explained with the above mentioned theoretical calculations results: HOMO-LUMO gap for **B2** and **L2** resulted on 3.07 and 2.75 eV, respectively. Therefore, since the gap for **B2** is higher than for **L2**, thus oxidation processes for the **B2** would require a larger energy input, i.e. oxidations potentials for **B2** shifted to more positive values were observed.

### 3.3 Preliminary Mercury (II) determination used 2,4-di-tert-butyl-6-(3H-imidazo[4,5-c]pyridine-2-yl)phenol (**B2**).

Since **B2** exhibited absorption and emission properties, we wanted to determine whether the presence of Hg (II) could produce a quenching effect of fluorescence. When excited at 330 nm, the emission spectrum displayed by **B2** in ethanol and in acetonitrile was 507 nm and 500 nm, respectively. We observed that the fluorescence intensity consistently decreased in presence of increasing amounts of Hg(NO<sub>3</sub>)<sub>2</sub> in solution, as shown in Figure 7. This quenching effect can be explained by a coordination between the metal and **B2**. This coordination possibly involves the hydroxyl groups and the nitrogen of -C=N in the benzimidazole ring, as previously described for similar compounds that possessed heteroatoms.<sup>67-71</sup> On the other hand, we observed that Cd(II) exerted no quenching effects of the **B2** fluorescence, as well as other anions such as sulfates, chlorides or nitrates (data not shown).

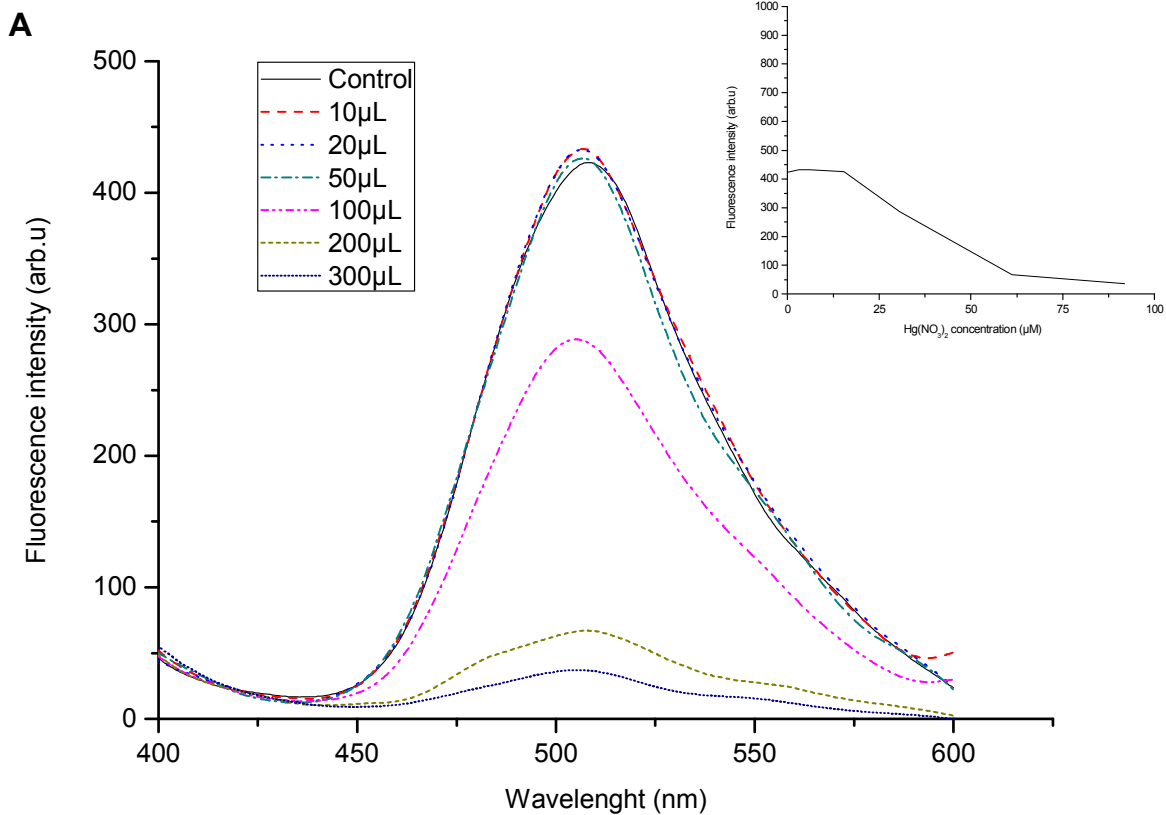


**Figure 7.** The presence of increasing amounts of Hg(NO<sub>3</sub>)<sub>2</sub> in aqueous solution, decrease fluorescence intensity of **B2**. Solvent: Ethanol.

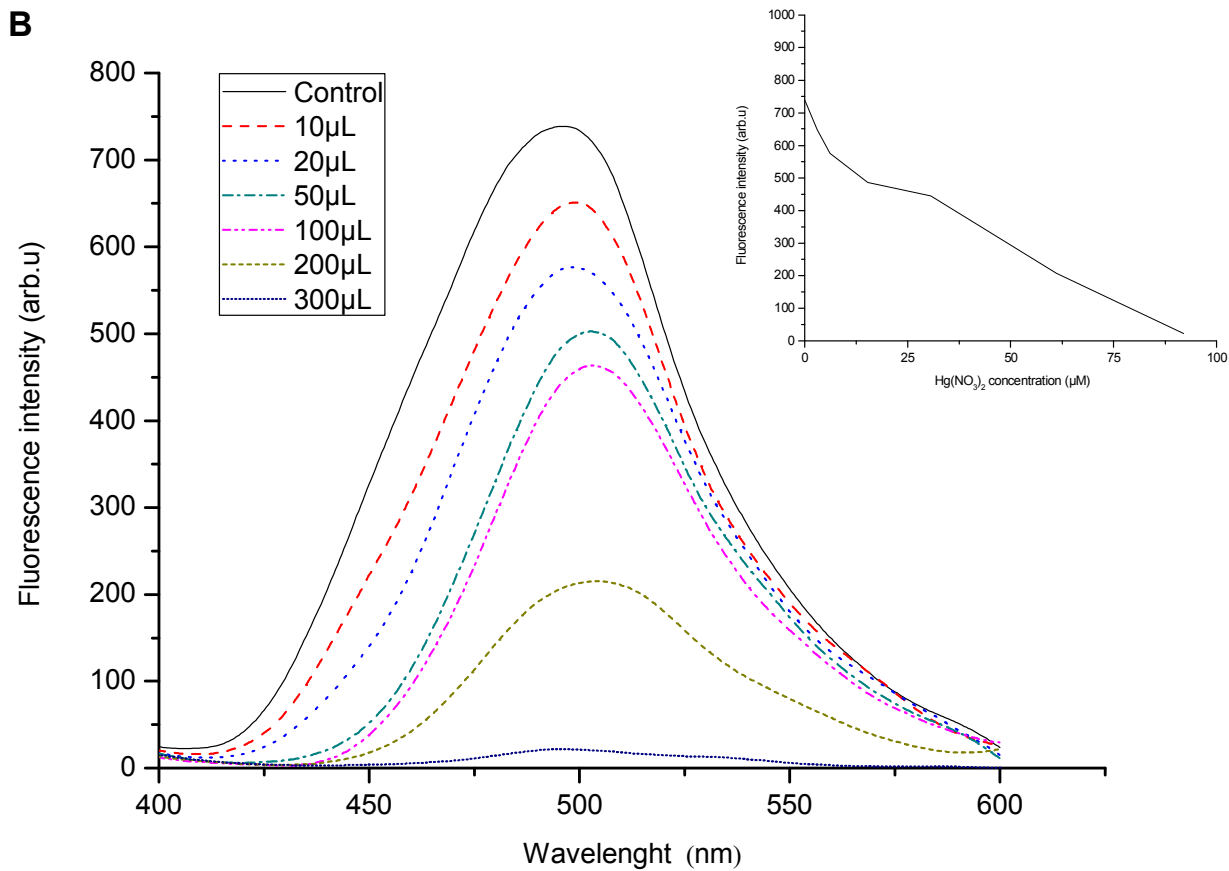


**Figure 8.** The presence of increasing amounts of Hg(NO<sub>3</sub>)<sub>2</sub> in aqueous solution, decrease fluorescence intensity of **B2**. Solvent: Acetonitrile.

### 3.4 Antifungal activities

#### 3.4.1 Compound 2,4-di-tert-butyl-6-(3H-imidazo[4,5-c]pyridine-2-yl)phenol (**B2**) exhibit antifungal activity against *Cryptococcus* spp.

We recently reported that (*E*)-2-{[(3-aminopyridin-4-yl)imino]-methyl}-4,6-di-tert-butyl-phenol (**L2**) exhibited antifungal properties against yeasts.<sup>32</sup> In order to test the potential antimicrobial activity of 2,4-di-tert-butyl-6-(3H-imidazo[4,5-c]pyridine-2-yl)phenol (**B2**), we determined the minimal inhibitory concentration (MIC) against clinical strains of *Cryptococcus* spp., *Candida albicans*<sup>72</sup> and *Candida tropicalis*,<sup>73</sup> yeasts involved in opportunistic infections in humans,<sup>74</sup> some of them with death risk. In addition, we also determined the MIC against *Salmonella enterica* (*S. enterica*),<sup>75</sup> a bacterial pathogen involved in gastroenteritis in humans.<sup>76</sup> We used **L2**<sup>32</sup> to compare its antimicrobial effects with **B2**. Considering that compounds with low MIC exhibit better antimicrobial activity, we observed that the strain of *Cryptococcus* spp.<sup>77</sup> used in this work was resistant to two commercial antifungal compounds used as control (**K1** and **K2**),<sup>78,79</sup> whereas the two *Candida* species tested were resistant to **K2**.<sup>80</sup> We have previously reported that the *Cryptococcus* spp. strain used in this study is resistant to **K1**<sup>32</sup> Furthermore, *Cryptococcus* spp. and *Candida* spp. strains resistant to **K1** and/or **K2** have also been previously disclosed<sup>81</sup>, supporting our results. On the other hand, as well as with **L2**, **B2** exhibited antifungal properties only against *Cryptococcus* spp., and not against *Candida* spp., albeit **B2** appeared to be less effective than **L2** (Table 6). In the case of bacteria, we observed antimicrobial effects only with chloramphenicol (**C1**, control), since neither **L2** nor **B2** presented antibacterial properties under the tested conditions.<sup>32</sup>

To determine the antifungal effect of **B2** in an independent way, we performed a modification of the disk diffusion assay (see Materials and Method). Figure 10 shows that the inhibition growth halo obtained with **B2** are evidently larger than the inhibition growth halo obtained with DMSO alone (control), but smaller than the halo obtained with **L2** when *Cryptococcus* spp. was tested, supporting the observations with the MICs. In the case of *Candida albicans* and *Candida tropicalis*, neither **B2** nor **L2** exhibited significant growth inhibition halos compared with the DMSO alone, as expected from the MICs (Figure 9). From these experiments, we conclude that **B2** exhibited antifungal activity against *Cryptococcus* spp.

**Table 6.** Minimal inhibition concentration (ppm) of tested compounds.<sup>a</sup>

Compound	Bacteria	Yeasts		
	<i>Salmonella enterica</i>	<i>Cryptococcus spp.</i>	<i>Candida albicans</i>	<i>Candida tropicalis</i>
<b>C1</b>	3.125 ± 0.156	ND	ND	ND
<b>L2</b>	-	4.468 ± 0.022	-	-
<b>B2</b>	-	6.625 ± 0.033	-	-
<b>K1</b>	ND	-	0.746 ± 0.037	0.746 ± 0.037
<b>K2</b>	ND	-	-	-

<sup>a</sup>The inhibition was indistinguishable from the vehicle (DMSO) alone

ND: Not determined

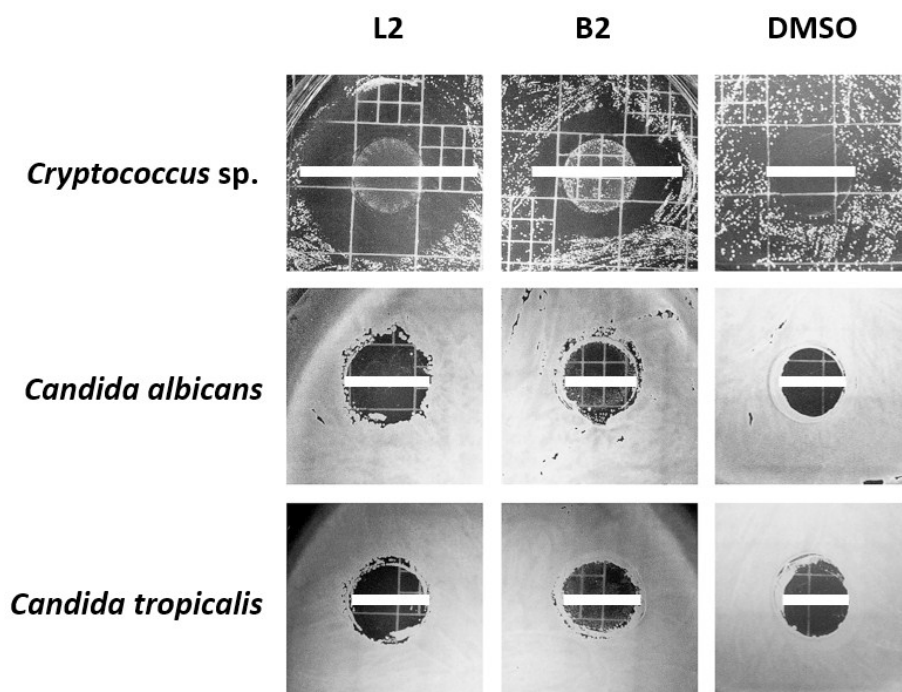


**Figure 9.** Inhibition growth halos of *Cryptococcus* sp., *Candida albicans* and *Candida tropicalis* in presence of **L2**, **B2**, and DMSO (control). The white horizontal lines delimit the inhibition growth halos. The diameters of inhibition halos are the following (cm). For *Cryptococcus* sp.: **L2** =  $1.55 \pm 0.04$ ; **B2** =  $1.16 \pm 0.05$ ; DMSO =  $0.84 \pm 0.01$ ; for *Candida albicans*: **L2** =  $0.75 \pm 0.01$ ; **B2** =  $0.61 \pm 0.01$ ; DMSO =  $0.56 \pm 0.02$ ; for *Candida tropicalis*: **L2** =  $0.68 \pm 0.03$ ; **B2** =  $0.61 \pm 0.01$ ; DMSO:  $0.67 \pm 0.01$ .

### 3.4.2 *Botrytis cinerea* B05.10

We also tested the antimicrobial activities of **B2** and **L2** against *Botrytis cinerea*, a ubiquitous plant pathogen. We observed that both **B2** and **L2** were able to inhibit growth of *Botrytis cinerea* strain B05.10<sup>82</sup> in a dose-dependent fashion. When these compounds were applied to low doses, 2 and 4 ppm, there was no significant decrease in growth. However, when doses of 8 and 10 ppm were used, the compounds were able to significantly inhibit the growth of this fungus. The range of concentrations used is according to the effective concentrations reported for the commercial fungicide fenhexamide. Two ppm of Fenhexamide were sufficient to significantly inhibit the growth of *Botrytis cinerea* B05.10 under the tested conditions (data not shown). Therefore, both **B2** and **L2** acted as antifungal

compounds against *Botrytis cinerea* in similar concentrations than fenhexamide, the most used commercial fungicide used against this pathogenic fungus (Figure 10).

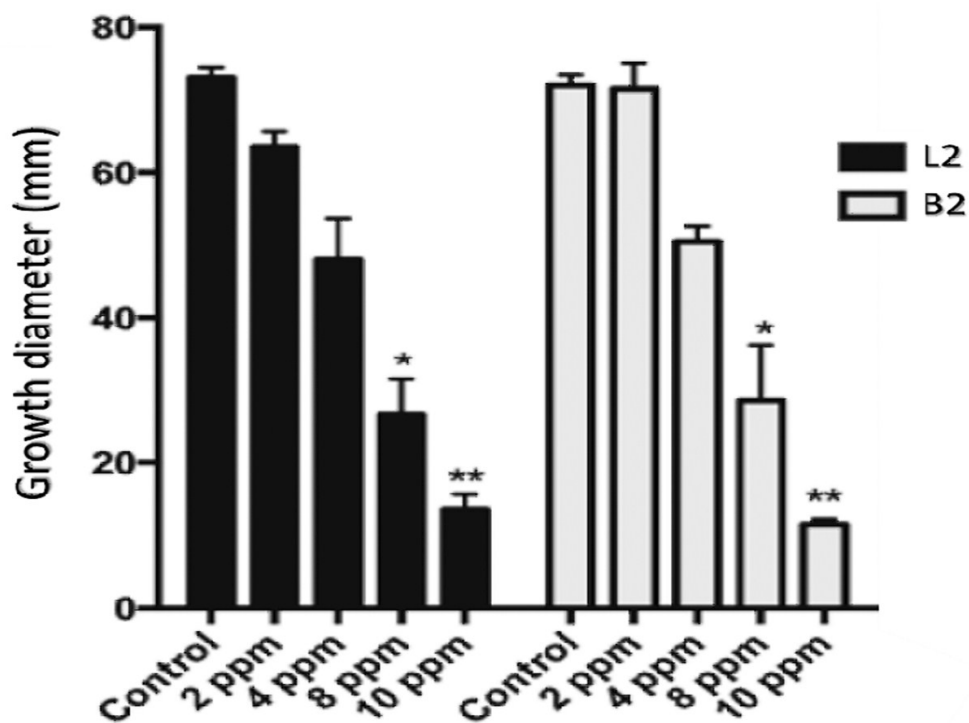


**Figure 10.** Effect of 2,4-di-*tert*-butyl-6-(3H-imidazo[4,5-c]pyridine-2-yl)phenol (**B2**) and (*E*)-2-[(3-aminopyridin-4-yl)imino]-methyl}-4,6-di-*tert*-butyl-phenol (**L2**) on *in vitro* growth of *Botrytis cinerea* B05.10. **B2** was added on potato dextrose agar (PDA) plates at doses of 2, 4, 8 and 10 ppm. The mycelial growth was measured until the fungus reached its maximum growth on control plate. Bars represent average value of the diameter of growth. The vertical lines represent the standard deviation. n = 2. \*p < 0.5; \*\*p < 0.05.

### 3.5 Cellular uptake studies

During the course of this study, we realized that 2,4-di-*tert*-butyl-6-(3H-imidazo[4,5-c]pyridine-2-yl)phenol (**B2**) remained somehow “attached” to cells, retaining its luminescence. When *Salmonella enterica* were mixed with **B2**, we observed that bacteria remained fluorescent even after 4 washes with phosphate buffer solution (PBS)<sup>83</sup> (Figure 11A). To determine whether the bacterial concentration can affect the amount of **B2** retained by the cells, we mixed different concentrations of *S. enterica* with one volume of **B2**, prior to obtaining the supernatants and the bacterial pellets. The bacterial pellets were washed 4 times with PBS, and then resuspended in DMSO to recover the retained **B2**. At this point, bacterial pellets were discarded. As shown in Figure 11B, fluorescence detected in the supernatant is inversely proportional to the bacterial concentration, strongly suggesting that the bacterial removal is in turn removing **B2**. Conversely, fluorescence obtained from pellets is directly proportional to the bacterial concentration, confirming that **B2** is retained by bacteria.

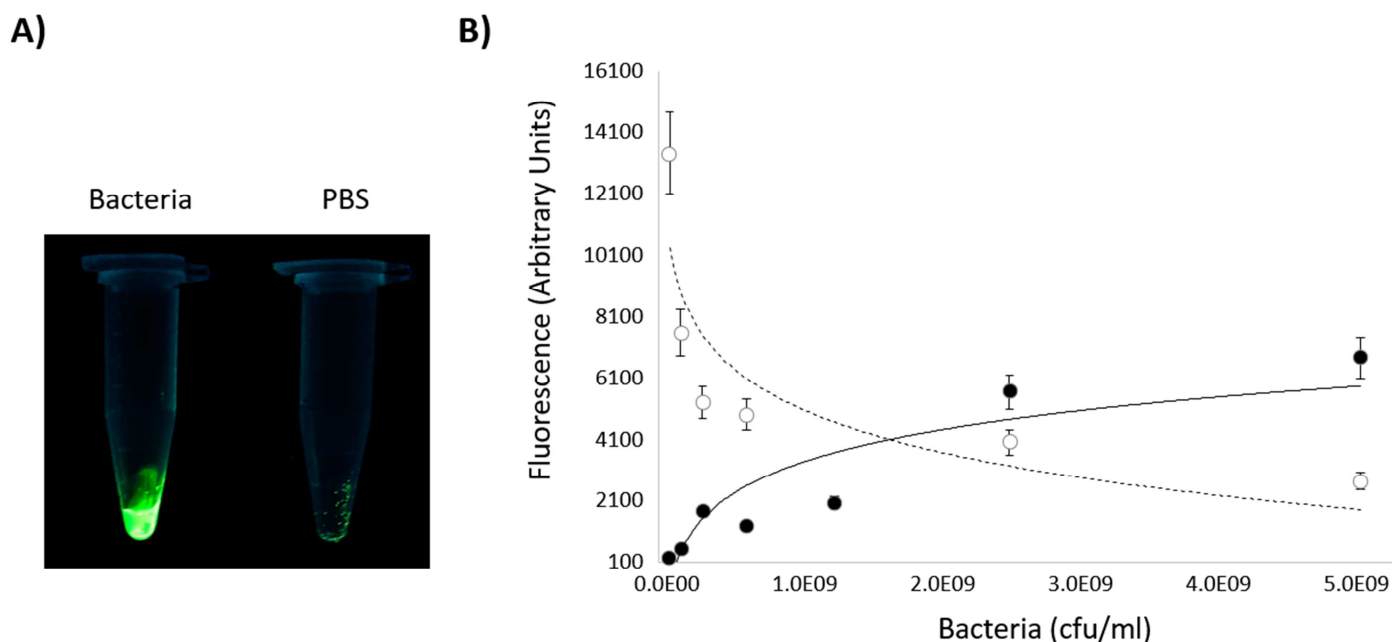


**Figure 11.** Fluorescence intensity of 2,4-di-*tert*-butyl-6-(3H-imidazo[4,5-c]pyridine-2-yl)phenol (**B2**) correlates with the amount of bacteria. A) *S. enterica* in phosphate buffer solution (PBS) ( $5 \times 10^9$  cfu/ml) was mixed with one volume of **B2** (400 ppm in DMSO) prior to incubating 5 min at 37 °C. As control, PBS alone was used instead of bacteria. After the incubation, bacteria were washed 4 times with PBS, and finally resuspended in PBS. Fluorescence was revealed by placing the tubes in a UV transilluminator (Excitation: 312 nm). B) Different concentrations of bacteria (*S. enterica*) in phosphate PBS were mixed with one volume of **B2** (100 ppm in DMSO). The mixture was incubated 5 min at 37 °C and centrifuged. Supernatant was collected and the fluorescence (excitation: 350 nm; detection: 500 nm) was measured. The corresponding bacterial pellets were subsequently washed 4 times with PBS prior to being resuspended in DMSO to recover the retained **B2**. At this point, the bacterial pellet was discarded. Fluorescence intensity (excitation: 350 nm; detection: 500 nm) in recovered **B2** from bacteria was determined. White circles: Fluorescence detected in supernatant. Black circles: Fluorescence detected in recovered **B2** from bacterial pellet. Dashed line: Trend line for fluorescence in supernatant. Continuous line: Trend line for fluorescence in bacterial pellet.

All the results shown in Figure 11, along with the promising photophysical properties of the 2,4-di-*tert*-butyl-6-(3H-imidazo[4,5-c]pyridine-2-yl)phenol (**B2**) described above, prompted us to perform fluorescent microscopy assays using confocal microscopy. As a first approach, we assessed the potential of **B2** to stain bacteria. For that, *S. enterica* was mixed with **B2**, incubated 5 min at 37 °C, and washed 4 times with PBS. Fresh samples were observed with the confocal microscope with an objective of 100x.<sup>84</sup> DMSO alone, instead of **B2**, was used to set the detection threshold. As shown in Figure 12A, **B2** fluorescence can be efficiently used to detect *S. enterica*, demonstrating that **B2** is indeed uptaken by bacteria. To unequivocally determine that **B2** is retained by bacteria, we used *Escherichia coli*/pGLO. *Escherichia coli*/pGLO constitutively expresses the green fluorescent protein (GFP), a useful mark to determine the exact position of bacteria. As shown in Figure 13B, the fluorescence associated to **B2** correlates almost perfectly with the green fluorescence of the GFP. As usual, some bacteria are not expressing GFP. Nevertheless, they are clearly revealed by **B2** (Figure 12B). As a next step, we wanted to assess whether **B2** is suitable to stain eukaryotic cells. For that, we first used *Candida albicans*.<sup>85</sup> Yeasts were mixed with **B2** and washed 4 times, following the same procedure described for bacteria, prior to being observed with the confocal microscope. Unexpectedly, we observed that *Candida albicans* is autofluorescent, emitting in the range of UV (data not shown). At this point, the control with DMSO was very useful to accurately set the threshold of detection. As shown in Figure 12A, yeasts uptook **B2**, showing that this compound can be used as a new fluorescent dye for both prokaryotic and walled eukaryotic cells.

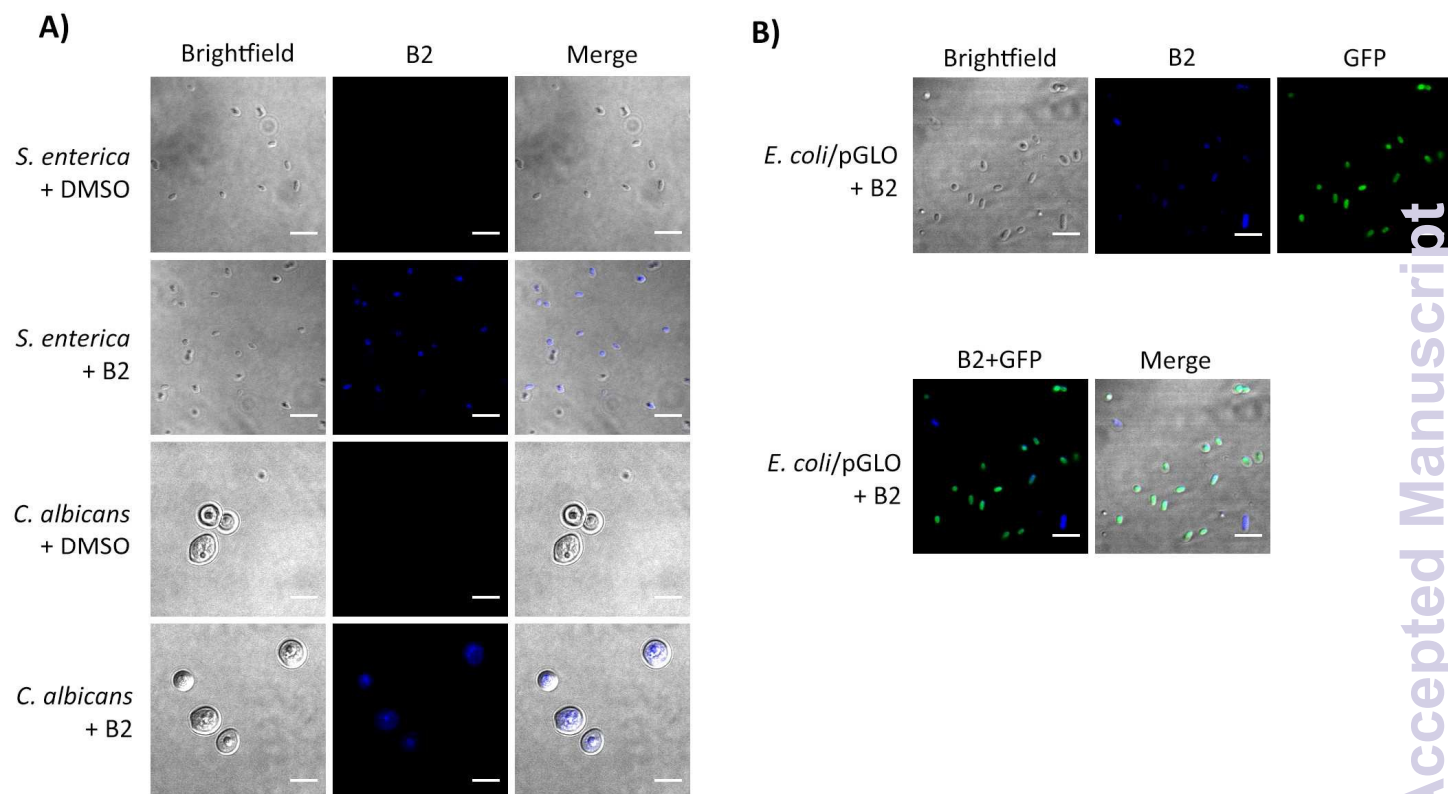


**Figure 12.** Fluorescence confocal microscopy images showing bacteria (*Salmonella enterica*) and yeasts (*Candida albicans*) (A) or bacteria constitutively expressing GFP (*Escherichia coli/pGLO*) (B). In all the cases, the microorganisms were observed fresh, using a 100X objective. White bars represent 5  $\mu\text{m}$ . DMSO alone was used to set the detection threshold.

To further assess whether 2,4-di-*tert*-butyl-6-(3H-imidazo[4,5-c]pyridine-2-yl)phenol (**B2**) can be used to detect and stain other eukaryotic cells, we tested **B2** for preliminary cell microscopy studies using a human ovarian cancer cell (SKOV-3).<sup>86</sup> Our results showed the suitability of our compound for cell microscopy applications. Fluorescent images (Figure 13) clearly showed a punctuate distribution of exogenous **B2** compound. Cellular uptake of this compound was efficient, showing a characteristic distribution as punctuated endosomes, whereas nuclear membrane seems to be impermeable to our compounds.<sup>87,88</sup> Distribution of this compound is similar in an embryonic kidney cell line HEK-293 (see Figure S14, ESI<sup>†</sup>) showing no difference between a cancer cell and a healthy one (data not shown). All these results together clearly demonstrate that **B2** is a suitable compound to stain cells, including bacteria, yeasts, and other eukaryotic cells, including human cells.

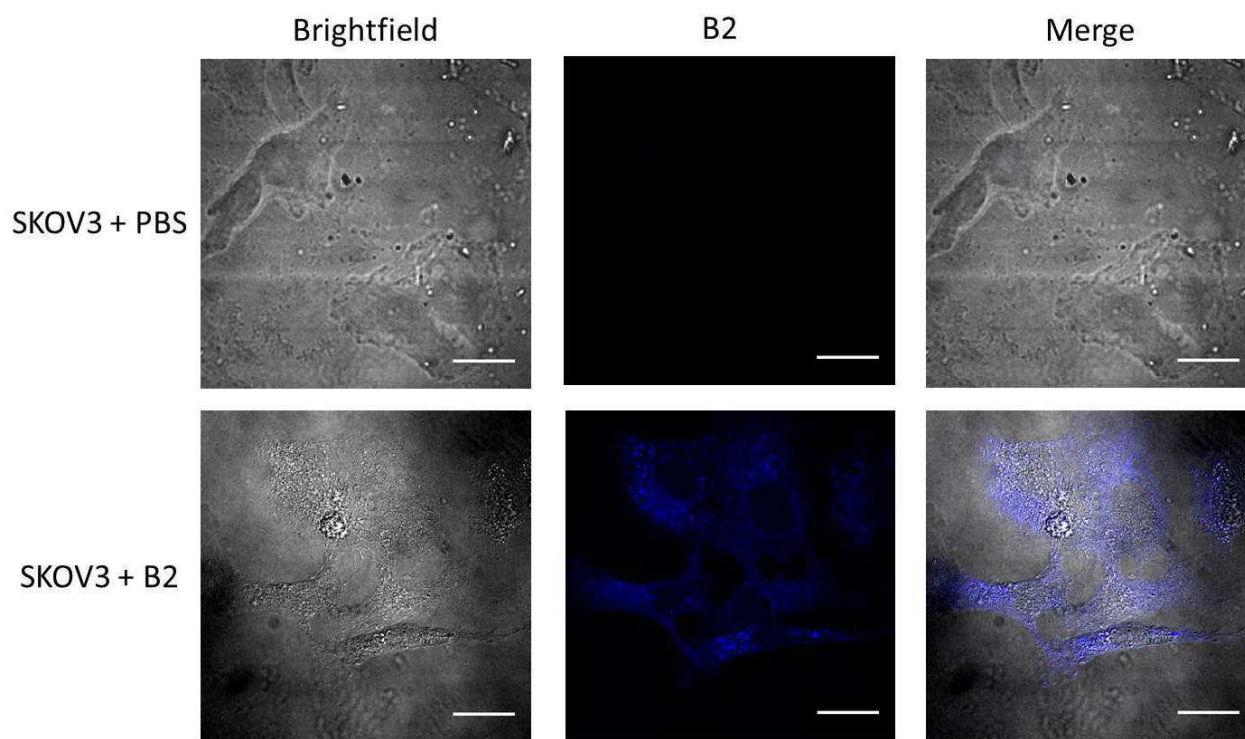


**Figure 13.** Fluorescence confocal microscopy images showing SKOV3 cells fixed after treatment with 2,4-di-*tert*-butyl-6-(3H-imidazo[4,5-c]pyridine-2-yl)phenol (**B2**), 50  $\mu$ M for 15 minutes. In all cases, cells were observed using a 100X objective. Compound emission was observed between 425-525 nm. White bars represent 10  $\mu$ m.

#### 4. Conclusions

In the present work, we reported a conventional synthesis of a new kind of pyridine benzimidazole [2,4-di-*tert*-butyl-6-(3H-imidazo[4,5-*c*]pyridine-2-yl)phenol; (**B**)] that possesses an intramolecular hydrogen bond. In addition, we fully characterized **B2** regarding several properties by different approaches, including experimental and computational studies. The main focus of the present manuscript is not the synthesis procedure of **B2**, but the characterization of different chemical and biological applications of **B2**. From the chemical point of view, the most interesting properties found in **B2**, including the fluorescence and the electrochemical profile, can be attributed to the presence of the intramolecular hydrogen bond as assessed by both experimental and theoretical studies, demonstrating that the quantum chemical studies are correctly set.

The electronic and electrochemical properties of **B2** were described and compared with (*E*)-2-[(3-aminopyridin-4-yl)imino]-methyl}-4,6-di-*tert*-butyl-phenol (**L2**). The presence of the intramolecular hydrogen bond of **B2** was confirmed by <sup>1</sup>HNMR showing a strong peak at approximately 13.6 ppm in DMSO-*d*<sub>6</sub>, similar to observed by **L2**. Also, UV-vis spectra in different solvents showed no band-shift, confirming the stability of this hydrogen bond.

The electrochemistry studies showed that 2,4-di-*tert*-butyl-6-(3H-imidazo[4,5-*c*]pyridine-2-yl)phenol (**B2**) exhibited two irreducible oxidation processes attributed to NH and -OH groups and irreducible reduction processes due to the reduction of the -C=N- group, and involves a self-protonation reaction at -1.28 V. Moreover, **B2** exhibited a quasireversible reduction process at  $E_{1/2} = -0.84$  V vs SCE attributed to a proton transfer from the phenol moiety to the bulk of the solution what not observed for **L2**.

The characters of the UV-Vis bands were described by means of TD-DFT calculations. The stability of the hydrogen bond was also confirmed by the character of the absorption band, where the band is located experimentally around 370 nm in all solvents. Theoretically this band is associated with a HOMO→LUMO transitions, where the -OH groups is involved. We have observed that **B2** the major contribution to the HOMO is located in the phenolic rings harboring the intramolecular hydrogen bond. By contrast, the HOMO distribution of **L2** is found in both the pyridine and the phenolic ring.

On the other hand, in the case of **B2**, the intramolecular hydrogen bond plays an important role in the luminescence properties because gives rigidity in both benzimidazole and hydroxyl rings. The model

2,4-Di-*tert*-butyl-1-methoxy-benzene (compound with 2-methyl-3H-imidazo[4,5-c]pyridine) (**B3**) used in the computational approach showed that when the hydrogen bond is broken the molecule adopt a twist configuration with an increment in the dihedral angle between rings. It means that similarly to **L2** the emission properties in the **B2** compound is a consequence of the rigidity of the structure due to the intramolecular H-bond.<sup>32</sup>

We have also shown that 2,4-di-*tert*-butyl-6-(3H-imidazo[4,5-c]pyridine-2-yl)phenol (**B2**) exerted an antifungal effect against both *Cryptococcus* spp. and *Botrytis cinerea*. Nevertheless, **B2** exhibited no antimicrobial effects against bacteria or other yeasts, including *Candida* spp. In addition, (*E*)-2-[(3-aminopyridin-4-yl)imino]-methyl}-4,6-di-*tert*-butyl-phenol (**L2**) appears to be a better antifungal compound compared with **B2**, when *Cryptococcus* spp. was assessed.

The 2,4-di-*tert*-butyl-6-(3H-imidazo[4,5-c]pyridine-2-yl)phenol (**B2**) compound showed a quenching fluorescence in presence of aqueous Hg(II) in acetonitrile or ethanol solvents essays. Moreover, because of its fluorescent property, **B2** has proven to be suitable as a new fluorescent dye to detect bacteria (*Salmonella enterica* and *Escherichia coli*/pGLO), yeasts (*Candida albicans*),<sup>87</sup> human cells (HEK-293 and SKOV-3) by confocal microscopy,<sup>88-91</sup> and it can be used as a dye for both prokaryotic and walled eukaryotic cells. Further research will be necessary to fully exploit these favorable features in order to develop sensors and new molecular biomarkers.

**Supporting Information:** Supplementary data associated with this article can be found, in the online version.

### **Acknowledgment**

This work has been funded by Project RC120001 of the Iniciativa Científica Milenio (ICM), FONDECYT 11140294, 1150629, 11121506; Guido A. Mora thanks Núcleo UNAB Grant DI-22-12/N. We are grateful to Dr. Maria A. Del Valle (PUC) and Dr. Luis Velasquez (CIMIS) for instrumentals facilities; Dr. Marcelo Preite (PUC) and Monique Riviere-Baudet (U. Paul Sabatier, France) for valuable NMR and Mass spectra discussions; Dr. Gerald. J. Meyer (University of North Carolina at Chapel Hill, USA) for photophysical measurement; B.Sc. Miriam Barros (Confocal microscopy, UNAB) and B.A. Alfonso Inzunza G. for his help with the English translation.

## References

1. X. Wang ; L. Wei ; L.P. Kotra; *Bioorg. Med. Chem.*, 2007, **15**, 1780.
2. A. Husain ; M.M. Varshney; M. Rashid; R. Mishra ; A. Akhter ; *J. Pharm. Res.*, 2011,**4**, 413.
3. P. Olliaro ; J. Seiler ; A. Kuesel ; J. Horton ; J.N. CFLark ; R. Don .; J. Keiser ; *Plos Neglected Tropical Diseases*, 2011, **5**, e1138.
4. J.B. Moreira ; J. Mann ; S. Neidle ; T.D. McHugh ; P.W. Taylor; *International Journal of Antimicrobial Agents*, 2013, **42**, 361
5. A. Tavman; S. Ikiz; A. F. Bagcigil; , N. Y. Ozgur; S. Ak; *Bull. Chem. Soc. Ethiop.*, 2010, **24**, 391
6. T. Lam; M. T. Hilgers; M. L. Cunningham; B. P. Kwan; K. J. Nelson; V. Brown-Driver; V. Ong; M. Trzoss; G. Hough; K. J. Shaw; J. Finn, *J. Med. Chem.*, 2014, **57**, 651
7. L. Srikanth ; V. Raj Varun ; N. Raghunandan ; L. Venkateshwerlu ; *Der Pharma Chemica*, 2011, **3**, 172.
8. J.D. Geratz ; F.M. Stevens; K.L. Polakoski; R.F. Parrish ; *Arch. Biochem. Biophys.* 1979, **197**, 551.
9. Fairley T.A.; Tidwell R.R.; Donkor I.; Naiman N.A.; Ohemeng K.A.; Lombardy R.J.; Cory M., *J. MedChem.* 1993, **36**, 1746.
10. B. George ; E.P. Papadopoulos ; *J. Org. Chem.* 1977, **42**, 441.
11. H. Fujioka ; K. Murai ; Y. Ohba ; A. Hiramatsu ; Y. Kita ; *Tetrahedron Lett.* 2005, **46**, 2197.
12. S. Peddibhotla ; J.J. Tepe ; *Synthesis* 2003, 1433.
13. J.M. Mitchell ; N.S. Finney ; *Tetrahedron Lett.* 2000, **41**, 8431.
14. S.L. You; J.W. Kelly ; *Org. Lett.* 2004, **6**, 1681.
15. V.A. Mamedov ; A.M. Murtazina ; *Chem. Rev.* 2001, **80**, 397.
16. S.V. Ryabukhin ; A.S. Plaskon ; D.M. Volochnyuk ; A.A. Tolmachev; *Synthesis* **2006**, 21, 3715.
17. D.W. Robertson ; J.H. Krushinski ; G. Don Pollock ; J. Scott Hayes; *J. Med. Chem.* 1988, **31**, 461.
18. A. El Nahhas ; A. Cannizzo ; F. van Mourik ; A.M. Blanco-Rodriguez ; S. Zalis; A. Vicek Jr.; M.

- Chergui ; *J. Phys. Chem. A*. 2010, **114**, 6361.
19. D.W. Robertson ; E. Beedle ; E. Krushinski ; G. Don Pollock ; H. Wilson ; V.L. Wyss ; J.S. Hayes ; *J. Med. Chem.* 1985, **28**, 717.
20. L. Benisvy ; A.J. Blake ; D. Collison ; E. Stephen Davies ; C.D. Garner ; E.J.L. McInnes ; J. McMaster ; G. Whittaker ; C. Wilson ; *Chem. Commun*, 2001, 1824.
21. L. Benisvy ; A.J. Blake ; D. Collison ; E.S. Davies ; C.D. Garner ; E.J.L. McInnes ; J. McMaster ; G. Whittaker ; C. Wilson ; *Dalton Trans.* 2003, 1975.
22. G. Kodis ; Y. Terazono ; P. Liddell ; J. Andreasson ; M. Hambourger ; T. Moore , A. Moore ; D. Gust ; *J. Am. Chem. Soc.* 2006, **128**, 1818.
23. G.F. Moore ; M. Hambourger ; M. Gervaldo ; O.G. Poluektov ; T. Rajh ; D. Gust ; T.A. Moore ; A.L. Moore ; *J. Am. Chem. Soc.* 2008, **130**, 10466.
24. A. Otavio ; T. Patrocinio ; N.Y. Murakami Ilha ; *Inorg. Chem.* 2008, **47**, 10851.
25. Y. Fuchs , S. Lofter , T. Dieter , W. Shi , R. Morgan , T.C. Streckas , H.D. Gafney , D. Baker ; *J. Am. Chem. Soc.* 1987, **109**, 9, 2691.
26. J. Costamagna, ; J. Vargas, ; R. Latorre, ; A. Alvarado, ; G. Mena; *Coord. Chem. Rev.* 1992, **119**, 67.
27. K.C. Gupta; A.K. Sutar.; *Coord. Chem. Rev.* 2008, **252**, 1420.
28. A. Prakash; D. Adhikari; *Int. J. Chem. Tech Res.* 2011, **3**, 1891.
29. M. Holbach, ; X. Zheng, ; C. Burd; C.W. Jones; M. Weck; *J. Org. Chem.* 2006 , **71**, 2903.
30. E. Kormaly; E. Kylic; *Talanta* 2002, **58**, 793.
31. A.R. Fakhari; A.R. Khorrami; H. Naeimi; *Talanta* 2005, **66**, 813.
32. A. Carreño ; M. Gacitua ; D. Paez-Hernandez ; R. Polanco ; M. Preite ; J.A, Fuentes ; G.C. Mora; I. Chavez ; R. Arratia-Perez; *New Journal of Chemistry*, 2015, **39**, 5725
33. D. Paez-Hernandez; J. Murillo-Lopez; R. Arratia-Perez, *Organometallics*, 2012, **31**, 5648

34. A. Carreño; A. Vega; X. Zarate; E. Schott; M. Gacitua; N. Valenzuela; M. Preite; J.M. Manriquez; I. Chavez, *Quim. Nova*, 2014, **37**, 584
35. A.E. Kalamarakis ; N. Petsikos-Anagiotarou; B. Mavroidis; N. Ziogas; *J. Phytopathology*, 2000, **138**, 449
36. B.A. Latorre ; C. Lillo ; M.E. Rioja; *Cien. Inv. Agr.*, 2001, **28**, 61
37. P. Elmer ; T. Reglinski ; *Plant Pathol*, 2006, **55**, 155
38. T.J. Michailides ; P.A.G. Elmer ; *Plant Disease*, 2000, **84**, 208
39. B. Williamson ; B. Tudzynsky ; P. Tudzynsky ; J.A.L. Van Kan ; *Mol Plant Pathol*, 2007, **8**, 561
40. G.W. Moorman ; R.J. Lease ; *Plant Diseases*, 1992, 477
41. R.E. Beever ; J. Elvidge ; *New Zealand Journal of Agricultural Research*, 1986, **29**, 299
42. A.M. Seyfarth ; H.C. Wegener ; N. Frimodt-Møller, *Journal of Antimicrobial Chemotherapy*. 1997, **40**, 67
43. H.M. Chen<sup>H</sup> ; Y. WANG; L.H. SU ; C.H. CHIU ; *Pediatr Neonatol*, 2013, **54**, 147
44. L. Benisvy ; E. Bill ; A.J. Blake ; D. Collison ; E.S. Davies ; C.D. Garner ; C.I. Guindy ; E.J.L. McInnes; G. McArdle ; J. McMaster ; C. Wilson ; J. Wolowska ; *Dalton Trans.* 2004, 3647.
45. A. Carreño ; M. Preite ; J.M. Manriquez ; A. Vega ; I. Chávez ; *Acta Crys.* 2010, E66, o3290.
46. L. Benisvy ; A.J. Blake; D. Collison ; E.S. Davies ; D. Garner ; E.J.L. McInnes ; J. McMaster ; G. Whittaker ; C. Wilson ; *Chem. Commun*, 2001, 1824
47. G.A. Crosby; J.N. Demas,; *J. Phys. Chem.* 1971, **75**, 991
48. K. Nakamaru ; *Bull. Chem. Soc. Jpn.* 1982, **55**, 1639
49. Amsterdam Density Functional (ADF) Code; Vrije Universiteit: Amsterdam, 2007.
50. L. Verluise; T. Ziegler, *J. Chem. Phys.* 1988, **88**, 322
51. A.D. Becke, *J. Chem. Phys.* 1993, **98**, 5648
52. F. Kootstra; P.L. Boeij; J.G. Snijders, *J. Chem. Phys.* 2000, **112**, 6517

53. P. Romaniello; P.L. de Boeij, *Phys. Rev. B* 2005, **71**, 155108
54. R. Ramirez-Tagle; R. Arratia-Perez; *Chem. Phys. Lett.* 2009, **475**, 232
55. D.H. Waldeck, *Chem. Rev.* 1991, **91**, 415
56. T. Dziembowska; K. Ambroziak ; I. Majerz, *J. Mol. Struct.* 2005, **738**, 15
57. A. Ariffin ; N. Nordin ; W.A. Yehye; S.W. Ng ; *Acta Crys.* 2012, E68, o1605.
58. W. Schilf ; B. Kołodziej; E. Grech, *J. Mol. Struct.* 2006, **791**, 93
59. E. Tozzo; S. Romera; M.P. dos Santos; M. Muraro; R.H. Santos; L.M. Liao; L. Vizotto; E.R. Dockal, *J. Mol. Struct.* 2008, **876**, 110
60. O. Güngör; P. Gürkan, *J. Mol. Struct.* 2014, **107**, 62
61. S. Emamiam ; S.F. Tayyari ; *J. Chem. Sci.* 2013, **125**, 939
62. R.V. Gopal; A.M. Reddy; V.J. Rao, *J. Org. Chem.* 1995, **60**, 7966
63. R.T. Boere; T.L. Roemmele, *Coord. Chem. Rev.* 2000, **210**, 369
- 64 J. Lewinski; J. Zachara.; I. Justyniak; M. Dranka, *Coord. Chem. Rev.* 2005, **249**, 1185
- 65 F. Leyssner; S. Hagen ; L. Ovari; P. Tegeder, *J. Phys. Chem. C*, 2010, **114**, 1231
66. R. Sustmann ; W. Sicking ; M. Felderhoff ; *Tetrahedron*, 1990, **46**, 783
67. S. Zolezzi; E. Spodine; A. Decinti, *Polyhedron* 2002, **21**, 55
68. P. Neta ; J. Grodkowski ; *J. Phys. Chem.* 2005, **34**, 1
69. S.M. Sayyah ; M.M. El-Rabiey ; S.S. Abd El-Rehim ; R.E. Azooz ; *Journal of Applied Polymer Science*, 2006, **99**, 3093
70. H.J. Salavagione; J. Arias-Pardilla; J.M. Perez; J.L. Vazquez; E. Morallon; M.C. Miras; C. Barbero, *J. Electroanal. Chem.* 2005, **576**, 139
71. R.T. Bronson ; M. Montalti ; L. Prodi ; N. Zaccheroni ; R.D. Lamb ; N.K. Dally ; R.M. Izatt ; J.S. Bradshaw ; P.B. Savage; *Tetrahedron*, 2004, **60**, 11139
72. J.F. Callan ;, A. Prasanna de Silva ; D.C. Magri ; *Tetrahedron*, 2005, **61**, 8551

73. Y. Yu ; L.R. Lin ; K.B. Yang ; X. Zhong ; R.B. Huang ; L.S. Zheng ; *Talanta*, 2006, **69**, 10374.
74. D.X. West ;, A.E. Liberta; S.B. Padhye; R.C. Chilate; P.B. Sonawane; A.S. Kumbhar; R.G. Yerande; *Coord. Chem. Rev.*, 1993, **123**, 49
75. M. Cuenca-Estrella ; C.B. Moore ; F. Barchiesi ; J. Bille ; E. Chryssanthou; D. W. Denning; J. P. Donnelly; F. Dromer; B. Dupont; J. H. Rex; M. D. Richardson; B. Sancak; P. E. Verweij; J. L. Rodríguez-Tudela; *Clin. Microbiol. Infect*, 2003, **9**, 467
76. R. J. Kothavade; M. M. Kura; A. G. Valand; M. H. Panthak; *Journal of Medical Microbiology*, 2010, **59**, 873
77. A.T. Lord ; K. Mohadas ; S. Somanath ; S. Ambu ; *Ann. ClinMicrobiol. Antimicrob.*, 2010, **9**, 11
78. N. Ueno ; M.B. Lodoen ; *Curr. Opin. Microbiol.*, **2015**, 26, 53
79. J.W. Cheong ; J. McCormack ; *Med. Mycol*, **2013**, 51, 261
80. H. Vanden Bossche ; F. Dromer ; I. Improvisi ; M. Lozano-Chiu ; J.H. Rex ; D. Sanglard; *Med. Mycol*, **1998**, 36, 119
81. M. Arvanitis; T. Anagnostou; B.B. Fuchs; A.M. Caliendo; E. Mylonakis, *Clinical microbiology reviews*. **2014**, 27, 490
82. K. Ferreira-Paim; L. Andrade-Silva ; D.J. Mora; E. Lages-Silva; A.L. Pedrosa; P.R. da Silva et al., *Mycopathologia*. 2012, **174**, 41
83. A.J. Bava; R. Negroni., *Rev. Int. Med. Trop. S. Paulo*. 1989, 31, 346
84. M. Choquer ; E. Fournier ; C. Kunz ; C. Levis ; J.M. Pradier ; A. Simon ; M. Viaud ; *FEMS Microbiol Lett*, **2007**, 277, 1
85. M. Chandra ; *EMD, an affiliate of Merck KGaA*, Darmstadt, Germany
86. J. Parras-Rojas ; A.A. Moreno ; I. Mitina ; A. Orellana ; *Plos One*, 2015, **10**, 1
87. P. Staib ; M. Kretschmar ; T. Nichterlein ; H. Hof ; J. Morschhauser ; *PNAS*, 2000, **97**, 6102

88. C. van Haaften ; A. Boot ; W.E. Corver ; J.D.H. van Eendenburg ; B. J.M.Z. Trimbos ; T. van Wezel ; *Journal of Experimental & Clinical Cancer Research*, 2015, **34**, 38
89. G. Huang; *Fungal Genom Biol.* 2013, **3**, 1
90. J.B. Kaper; J.P. Nataro; H.L.T. Mobley; *Nature review; Microbiology*, 2004, **2**, 122
91. A. Lischewski; M. Kretschmar; H. Hof; R. Amann; J. Hacker; J. Morschhauser; *Journal of Clinical Microbiology*, 1997, **35**, 2943.

## Theoretical and experimental characterization of a novel pyridine benzimidazole: Suitability for fluorescence staining in cells and antimicrobial properties.†

Alexander Carreño<sup>1,2\*</sup>, Manuel Gacitúa<sup>3</sup>, Juan A. Fuentes<sup>8</sup>, Dayán Paez-Hernandez<sup>1,2</sup>, Carmen Araneda<sup>4</sup>, Ivonne Chávez<sup>4,2</sup>, Marco Soto-Arriaza<sup>5</sup>, Juan M. Manriquez<sup>6,2</sup>, Rubén Polanco<sup>7</sup>, Guido C. Mora<sup>9</sup>, Carolina Otero<sup>10</sup>, Wesley B. Swords<sup>11</sup>, Ramiro Arratia-Perez<sup>1,2</sup>

Imidazopyridine presenting an intramolecular hydrogen bond showed fluorescence properties suitable for imaging with both prokaryotic and eukaryotic cells.

